Circulation Research

ORIGINAL RESEARCH

Chronic Activation of Tubulin Tyrosination Improves Heart Function

Niels Pietsch, Christina Y. Chen, Svenja Kupsch, Lucas Bacmeister, Birgit Geertz, Marisol Herrera-Rivero, Bente Siebels, Hannah Voß, Elisabeth Krämer, Ingke Braren, Dirk Westermann, Hartmut Schlüter, Giulia Mearini, Saskia Schlossarek, Jolanda van der Velden, Matthew A. Caporizzo, Diana Lindner, Benjamin L. Prosser, Lucie Carrier

BACKGROUND: Hypertrophic cardiomyopathy (HCM) is the most common cardiac genetic disorder caused by sarcomeric gene variants and associated with left ventricular hypertrophy and diastolic dysfunction. The role of the microtubule network has recently gained interest with the findings that microtubule detyrosination (dTyr-MT) is markedly elevated in heart failure. Acute reduction of dTyr-MT by inhibition of the detyrosinase (VASH [vasohibin]/SVBP [small VASH-binding protein] complex) or activation of the tyrosinase (TTL [tubulin tyrosine ligase]) markedly improved contractility and reduced stiffness in human failing cardiomyocytes and thus posed a new perspective for HCM treatment. In this study, we tested the impact of chronic tubulin tyrosination in an HCM mouse model (*Mybpc3* knock-in), in human HCM cardiomyocytes, and in SVBP-deficient human engineered heart tissues (EHTs).

METHODS: Adeno-associated virus serotype 9–mediated TTL transfer was applied in neonatal wild-type rodents, in 3-week-old knock-in mice, and in HCM human induced pluripotent stem cell–derived cardiomyocytes.

RESULTS: We show (1) TTL for 6 weeks dose dependently reduced dTyr-MT and improved contractility without affecting cytosolic calcium transients in wild-type cardiomyocytes; (2) TTL for 12 weeks reduced the abundance of dTyr-MT in the myocardium, improved diastolic filling, compliance, cardiac output, and stroke volume in knock-in mice; (3) TTL for 10 days normalized cell area in HCM human induced pluripotent stem cell–derived cardiomyocytes; (4) TTL overexpression activated transcription of tubulins and other cytoskeleton components but did not significantly impact the proteome in knock-in mice; (5) SVBP-deficient EHTs exhibited reduced dTyr-MT levels, higher force, and faster relaxation than TTL-deficient and wild-type EHTs. RNA sequencing and mass spectrometry analysis revealed distinct enrichment of cardiomyocyte components and pathways in SVBP-deficient versus TTL-deficient EHTs.

CONCLUSIONS: This study provides the first proof of concept that chronic activation of tubulin tyrosination in HCM mice and in human EHTs improves heart function and holds promise for targeting the nonsarcomeric cytoskeleton in heart disease.

GRAPHIC ABSTRACT: A graphic abstract is available for this article.

Key Words: cardiomyopathy, hypertrophic ■ induced pluripotent stem cells ■ microtubules ■ myocardium

---

In This Issue, see p 887 | Meet the First Author, see p 888

Hypertrophic cardiomyopathy (HCM) is the most common inherited cardiac disease caused by mutations in several sarcomeric genes. *MYBPC3* (myosin binding protein C3) is the most frequently mutated gene.[1] HCM is associated with left ventricular (LV) hypertrophy, diastolic dysfunction, and increased interstitial fibrosis. Treatment of severe HCM with outflow tract obstruction is limited to surgical removal of septal tissue or catheter ablation.

The role of the microtubule network during progression of cardiac diseases has gained interest in recent years with the findings that microtubule detyrosination and associated cardiomyocyte stiffness are elevated in HCM and

---

Circulation Research is available at www.ahajournals.org/journal/res

Novelty and Significance

What Is Known?

- Microtubule tyrosination is driven by TTL (tubulin tyrosine ligase), while detyrosination is facilitated by a complex of vasohibin and SVBP (small vasohibin-binding protein).
- Microtubules increase in density and are more heavily detyrosinated in different heart diseases such as hypertrophic cardiomyopathy (HCM), impeding cardiomyocyte contractility.
- Acute reduction of microtubule detyrosination improved contractility in failing cardiomyocytes.

What New Information Does This Article Contribute?

- Chronic activation of microtubule tyrosination by adeno-associated virus (AAV)-TTL improved heart function in HCM *Mybpc3*-mutated mice by increasing ventricular compliance and cardiac output.
- Chronic TTL overexpression rescued hypertrophy in HCM *MYBPC3*-mutated patient-derived induced pluripotent stem cell cardiomyocytes.
- Chronic activation of microtubule tyrosination by SVBP deficiency in human induced pluripotent stem cell improved contractility in engineered heart tissues.

The microtubule network contributes to ventricular stiffening in a plethora of cardiac pathologies, which is conveyed by detyrosinated microtubules. Acute activation of α-tubulin tyrosination with TTL improved the function of isolated cardiomyocytes, but studies investigating the chronic modulation of the detyrosination cycle are lacking. To investigate this, we delivered AAV-TTL in a mouse model of HCM, which improved cardiac output 12 weeks after treatment by increasing ventricular compliance, translating into improved diastolic filling and normalized cardiac output. TTL normalized the increased microtubule detyrosination in HCM mice, increased transcript levels of tubulins and cytoskeleton components, but did not impose major changes on the proteome, assessed by RNA sequencing and mass spectrometry. We further found that activating tubulin tyrosination by TTL overexpression rescued hypertrophy of HCM patient-derived human induced pluripotent stem cell cardiomyocytes. We created a human induced pluripotent stem cell–derived cardiomyocyte model of strongly modulated microtubule detyrosination by CRISPR/Cas9 (clustered regularly interspaced short palindromic repeats/clustered regularly interspaced short palindromic repeat–associated protein 9)–mediated knockout of SVBP or TTL. SVBP-KO engineered heart tissues displayed higher force development and faster relaxation, while TTL-KO tissues exhibited reduced force development and prolonged relaxation. Thus, we provide the first evidence that chronically decreased microtubule detyrosination improves cardiomyocyte and heart function and is a feasible strategy for the treatment of HCM.

heart failure[2,3] (for reviews, see references[4–7]). The cycle of α-tubulin detyrosination/retyrosination consists in the catalytic removal and reincorporation of the last C-terminal tyrosine of α-tubulin. We have previously reported higher levels of detyrosinated microtubules (dTyr-MTs) in human and mouse models of HCM.[3,8] The TTL (tubulin tyrosine ligase) catalyzes the tyrosination, and the tubulin carboxypeptidase complex, composed of VASH (vasohibin; VASH1 or VASH2) and its chaperone, the SVBP (small VASH-binding protein), catalyzes the removal of the C-terminal tyrosine of α-tubulin. VASH1 is the major isoform in the human heart.[9] Recently, it was shown that an acute reduction of dTyr-MTs by TTL overexpression or *VASH1* knockdown markedly improved contractility and reduced stiffness in human failing cardiomyocytes[8,9] and thus posed a possible new perspective for the treatment of HCM.

In this study, we evaluated the impact of long-term adeno-associated virus serotype 9 (AAV9)–mediated TTL overexpression in neonatal and adult wild-type (WT) rodents and in 3-week-old homozygous *Mybpc3*-targeted knock-in (KI) mice that present with eccentric LV hypertrophy and both systolic and diastolic dysfunction.[10,11] Using a combination of approaches, we show that a long-term TTL overexpression lowered dTyr-MTs, improved contractility without affecting calcium transients in WT rat cardiomyocytes, and improved diastolic filling, compliance, stroke volume (SV), and cardiac output (CO) in KI mice. These data were supported by a normalization of cell hypertrophy after a 10-day TTL gene transfer in HCM human induced pluripotent stem cell (hiPSC)–derived cardiomyocytes and by SVBP deficiency in hiPSC-derived cardiomyocytes and engineered heart tissues (EHTs).

METHODS

Data Availability

Data sets, analysis, and study materials will be made available on request to other researchers for the purpose of reproducing

Nonstandard Abbreviations and Acronyms

AAV9	adeno-associated virus serotype 9
ACTN2	α-actinin-2
BW	body weight
Cas9	clustered regularly interspaced short palindromic repeat–associated protein 9
CLIP	CAP-Gly domain-containing linker protein
CO	cardiac output
CRISPR/Cas9	clustered regularly interspaced short palindromic repeats clustered regularly interspaced short palindromic repeat–associated protein 9
CYB5R1	cytochrome b5 reductase 1
dTyr-MT	detyrosinated microtubule
dTyr-tub	detyrosinated tubulin
EF	ejection fraction
EHT	engineered heart tissue
ET1	endothelin-1
FA	formic acid
GO	gene ontology
H3	histone H3
HCM	hypertrophic cardiomyopathy
hiPSC	human induced pluripotent stem cell
KI	knock-in
KO	knockout
LV	left ventricle
MAP	microtubule-associated protein
MS	mass spectrometry
MYBPC2	myosin-binding protein C2
MYBPC3	myosin-binding protein C3
MYBPC3het	heterozygous MYBPC3
MYBPC3ic	MYBPC3 isogenic control
PV	pressure/volume
RNA-seq	RNA sequencing
SSEA-3	stage-specific embryonic antigen 3
SV	stroke volume
SVBP	small vasohibin-binding protein
TNNT2	cardiac troponin T2
TTL	tubulin tyrosine ligase
VASH	vasohibin
WT	wild type

the results or replicating the procedures. All omics data have been made publicly available. The RNA-sequencing (RNA-seq) data have been deposited to RNA-seq data sets to National Center for Biotechnology Information (NCBI) Gene Expression Omnibus of the European Nucleotide Archive at European Molecular Biology Laboratory-European Bioinformatics Institute (EMBL-EBI) with the accession numbers GSE233851 for mice and GSE233852 for EHTs. The mass spectrometry (MS) proteomics data have been deposited to the ProteomeXchange consortium via the Proteomics Identification Database (PRIDE)[12] partner repository with the data set identifier PXD054236.

Animals

The investigation conforms to the guidelines for the care and use of laboratory animals published by the National Institutes of Health (publication No. 85-23, revised 1985). For studies in WT C57BL/6J mice and Sprague-Dawley rats, animal care and use procedures were approved and performed in accordance with the standards set forth by the University of Pennsylvania Institutional Animal Care and Use Committee and the Guide for the Care and Use of Laboratory Animals published by the US National Institutes of Health.

KI mice were generated previously,[10] and both KI and WT mice were maintained on a Black Swiss genetic background. The experimental procedures performed in KI and WT mice were in accordance with the German Law for the Protection of Animals and accepted by the Ministry of Science and Public Health of the City State of Hamburg, Germany (No. 074-19). KI and WT mice were bred and kept in the animal facility Zenti 3 at the University Medical Center Hamburg-Eppendorf. Breeding was performed considering various parameters such as replacement rate, breeding renewal rate, colony index, and penetrance, and were set and limited to a necessary level. The animals were kept under barrier conditions in air-conditioned rooms in open cages closed with a mesh lid. The number of animals (group keeping) per cage (type II long) and the equipment of the cages are in accordance with part B of the Directive 2010/63/EU. Animal husbandry complies with the legal husbandry requirements in all the aspects. The rooms are air-conditioned (>15× air exchange, room temperature between 20 and 24 °C, and 45%–65% relative humidity) and are subjected to a 12-hour light-dark cycle. The care and daily monitoring of the animals were performed by trained animal caretakers from the research animal facility. The animals had ad libitum access to food and water. The animals received a complete animal feed (phytoestrogen deficient, irradiated, 1328 P; Altromin) composed of vegetable byproducts, cereals, and minerals.

Human Samples

The patient with HCM carrying the *MYBPC3* (c.2308G>A; p.Asp770Serfs98X) genetic variant was recruited in the outpatient HCM clinic at the University Heart and Vascular Center Hamburg and provided written informed consent for genetic analysis and the use of skin fibroblasts.[13] All procedures were in accordance with the Code of Ethics of the World Medical Association (Declaration of Helsinki). The study was reviewed and approved by the Ethical Committee of the Ärztekammer Hamburg (PV3501).

Plasmid Constructs and AAV9 Particle Production

The TTL-IRES-dsRed (discosoma sp. red fluorescent protein) insert was cloned into an expression construct flanked by adeno-associated virus serotype 2 inverted terminal repeats containing a human *TNNT2* (troponin T2, cardiac type)

promoter, a chimeric intron, the Woodchuck Hepatitis Virus Posttranscriptional Regulatory Element (WPRE), and a rabbit β-globin poly A sequence (PENN.AAV.cTNT.TTL.IRES.dsRed; Figure S1A through S1D). AAV9 pseudotyped vector was generated by triple transfection of human embryonic kidney 293 (HEK293) cells and iodixanol purification (Penn Vector Core, University of Pennsylvania) as described previously.[14] Genome copy titer was determined using a droplet digital polymerase chain reaction–based method.[15]

The pGG2-*TNNT2-HA-TTL* and the pAAV-*TNNT2*-Empty plasmids (Figure S1E) were generated from the pGG2-*TNNT2*-Mut1 plasmid (VC206) by In-Fusion Cloning kit (Takara Clontech; 638945). In brief, the full-length hemagglutinin (HA)-tagged TTL was amplified from the HA-TTL-IRES-dsRed plasmid using PrimeStar GLX Polymerase (Takara Clontech; R050B) and ligated into the *Nhe*I (Neisseria mucosa heidelbergensis) and *Bam*HI (Bacillus amyloliquefaciens) restriction sites of VC206. The Empty plasmid was generated by amplification of the *TNNT2* promoter region from the VC206 plasmid and inserted into *Mlu*I (Micrococcus luteus) and *Hin*dIII (Haemophilus influenzae) restriction sites of pAAV-GFP (Cell Biolabs; AAV-400). After ligation, ampicillin-resistant clones were tested by enzymatic digestion for the presence of the insert, and 1 positive clone of each pGG2-*TNNT2-HA-TTL* and pAAV-*TNNT2*-Empty was sequenced. AAV9 pseudotyped vectors were generated by triple transfection of HEK293 cells with pGG2-*TNNT2-HA-TTL* or pAAV-*TNNT2*-Empty, pE8/9 (kindly provided by Julie Johnston, Penn Vector Core, University of Pennsylvania, PA), and pHelper encoding adenoviral helper functions (Cell Biolabs; VPK-402). Generation of recombinant AAV9 particles was performed as described previously.[16,17]

In Vivo *AAV9* Administration

Neonatal WT C57BL/6 mice received (subcutaneous injection) AAV9-TTL-dsRed at a dose of 1.75E11 or 9E11 vg/g at postnatal day 2 (Figure 1A). Neonatal Sprague-Dawley rats received AAV9-TTL-dsRed at a dose of 4.4E11 vg/g at P4 (pericardial injection; Figure 1E). Six-week-old WT C57BL/6 mice received 5.625E11 vg/g of AAV9-TTL-dsRed for 6 weeks (Figure S1B). Three-week-old WT and KI mice received AAV9 encoding either an empty cassette (AAV9-Empty) or HA-tagged TTL (AAV9-TTL) at a dose of 2.25E11 vg/g via systemic administration into the tail vein using a 30-G needle (Figure S1F).[16–18]

Isolation of Adult Mouse and Rat Ventricular Myocytes and Functional Assessment

Primary ventricular cardiomyocytes were isolated as described previously.[19] Briefly, the heart was removed from 6-week-old mice or rats anesthetized under isoflurane and retrograde-perfused on a Langendorff apparatus with a collagenase solution. The digested heart was then minced and triturated using a glass pipette. The resulting supernatant was separated and centrifuged at 17g to isolate cardiomyocytes, which were then resuspended in cardiomyocyte media for functional assessment. Elastic modulus was measured using nanoindentation (Piuma Chiaro; Optics11 Life, the Netherlands) as described previously.[20] Cardiomyocyte contractility and calcium transients were measured as described previously.[9]

Human iPSC-Derived Cardiomyocytes and EHT Contractility Measurements

A control hiPSC line carrying a monoallelic mTag-RFP-T-TUBA1B (tubulin alpha 1b; clone AICS-0031-035; Allen Institute for Cell Science, Seattle, WA) was expanded and used to create SVBP-knockout (KO) and TTL-KO hiPSC lines with CRISPR/Cas9 (clustered regularly interspaced short palindromic repeats/CRISPR–associated protein 9) technology. Two single guide RNAs (sgRNAs) were selected for each locus to create a large deletion (Figure S2A). Cells were nucleofected using the Amaxa 4D nucleofector (Lonza) with preannealed ribonucleoprotein complexes of sgRNAs and recombinant Cas9 (clustered regularly interspaced short palindromic repeat–associated protein 9) protein (Integrated DNA Technologies; 1081058), and single-cell clones were expanded and genotyped for successful homozygous deletions (Figure S2B). Clones with large homozygous deletions for each of the genes of interest underwent quality control in karyotyping (Figure S2C) by nCounter profiling (NanoString, Seattle), pluripotency validation by SSEA-3 (stage-specific embryonic antigen 3) staining (BD Biosciences; 560892; Figure S2D), and control for mycoplasma contamination. To ensure specific activity of the CRISPR/Cas9 system, the 10 most likely off-target loci were identified with crispor.tefor. net[21] and sequenced to assess genome integrity. No alterations were detected, indicating no unspecific activity of the CRISPR/Cas9 complex (data not shown). After expansion of the 3 hiPSC lines, cardiomyocytes were produced according to the monolayer protocol.[22] Reverse transcription quantitative PCR (RT-qPCR) was performed with RNA isolated from hiPSC-derived cardiomyocytes to ensure mRNA deficiency of the respective gene (Figure S2E and S2F). EHTs were cast from 2 to 6 independent batches of cardiomyocyte differentiation (TNNT2-positive cardiomyocytes, >85%) of the 3 hiPSC lines on standard silicone posts (0.28 mN/mm) or on stiffer silicone that induced afterload enhancement (0.8 mN/mm). Auxotonic contractions were measured until day 60 as described previously.[23–25]

We also used patient-derived heterozygous *MYBPC3* (MYBPC3het; UKEi070-A) and *MYBPC3* isogenic control (MYBPC3ic; UKEi070-A1) hiPSC lines that were previously created.[13] MYBPC3het and MYBPC3ic hiPSC-derived cardiomyocytes (3–4 batches of differentiation of triplicates) were transduced with AAV9-TTL or AAV9-Empty (multiplicity of infection [MOI], 100 000) for 10 days and treated with 100 nmol/L ET1 (endothelin-1; Sigma; 05233800) or vehicle (H$_2$O) the last 3 days as described previously.[26] Cardiomyocytes were then stained for α-actinin (Sigma; SAB2108642, 1:800) and N-cadherin (Sigma; C2542, 1:500), followed by the secondary antibodies Alexa Fluor 488 (mouse) and Alexa Fluor 546 (rabbit; Invitrogen; A11001, A11035, 1:800), and cell area was analyzed by confocal microscopy and ImageJ.

Echocardiographic Analysis in Mice

The number of required animals was based on assuming a variance of 20% (measurement inaccuracy and biological variability within a group) and an impairment of the main echocardiographic parameter, which is LV fractional area shortening to 65% of the initial value of the WT-Empty group in the KI-Empty, as well as an improvement through treatment to 85% of the
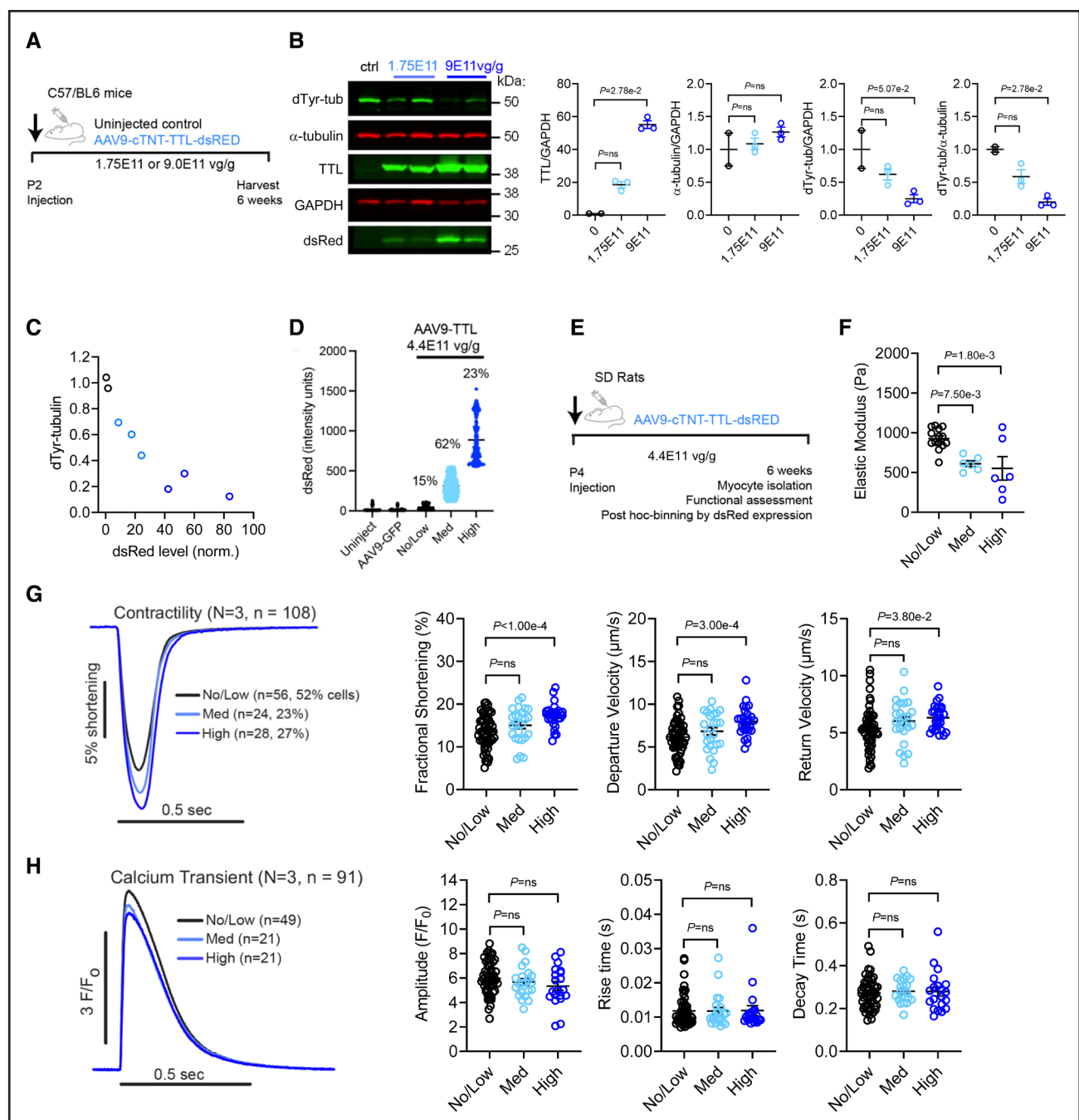
Figure 1. Effect of chronic *TTL* (tubulin tyrosine ligase) overexpression in wild-type rodents and analysis of isolated cardiomyocytes.

A, Protocol: wild-type neonatal male mice (postnatal day 2 [P2]) received either an adeno-associated virus serotype 9 (AAV9) encoding TTL-dsRed at a low (1.75E11 vg/g, N=3) or high dose (9E11 vg/g, N=3) or a sham injection (N=2). After 6 weeks, ventricular myocardium was harvested. **B**, Representative Western blot of crude proteins stained for detyrosinated tubulin (dTyr-tub), total α-tubulin, TTL, dsRed (Discosoma sp. red fluorescent protein), and GAPDH as a loading control, and quantification of TTL/GAPDH, α-tubulin/GAPDH, dTyr-tub/GAPDH, and dTyr-tub/α-tubulin; molecular weight units are given in kDa. **C**, Correlation between dsRed protein level (measured via Western blot) and dTyr-tub levels from the same hearts in **B**. **D**, Percentage of cardiomyocytes expressing no/low, medium, or high dsRed intensity after application of AAV9-TTL-dsRed of 4.4E11 vg/g in mice. **E**, Protocol: wild-type neonatal Sprague-Dawley rats (P4) received an AAV9 encoding TTL-dsRed at an intermediate dose (4.4E11 vg/g, N=3). After 6 weeks, single ventricular myocytes were isolated and functionally assessed. Following assessment, myocytes were binned into tertiles based on no/low, medium, or high level of TTL (indicated by dsRed fluorescence intensity). **F**, Myocyte stiffness (elastic modulus) measured via transverse nanoindentation. **G**, Sarcomere shortening representative traces and quantification of fractional shortening, contraction, and relaxation velocity. **H**, Calcium transient representative traces and quantification of amplitude, rise time, and decay time. Data are expressed as mean±SEM with N/n representing the number of analyzed mice and cardiomyocytes, respectively. Statistical significance was assessed with the Kruskal-Wallis test and Dunn multiple comparisons test (**B**) or with 1-way ANOVA and Dunnett multiple comparisons test (**F**–**H**). ns, $P>0.05$. N/n indicates number of analyzed mice and cardiomyocytes, respectively.

initial value in the KI-TTL group, a significance level of 0.05, and a statistical power of 0.95. This power calculation resulted in the required number of animals of 36. These animals were distributed evenly (N=12) among the 3 groups. The calculation was performed using the G-Power 3.1.7 software (University of Düsseldorf, Germany). Transthoracic echocardiography was performed using the Vevo 3100 System (VisualSonics, Toronto, Canada) as described previously.[16–18] After the last echocardiography, 11 mice remained per group (1 WT-Empty mouse died after the last echocardiography, 1 KI-Empty mouse died after the fourth echocardiography, and 1 KI-TTL mouse left the cage after the second echocardiography and was found dead).

Hemodynamic Measurements in Mice

Hemodynamic measurements were performed using a pressure/volume (PV) loop system (ADV500; Transonic) in closed-chest approach.[27,28] Mice (N=11 per group) were anesthetized using urethane (0.8–1.2 g/kg body weight [BW]) and buprenorphine analgesia (0.1 mg/kg BW), intubated, and artificially ventilated. A pressure-conductance catheter (1.2F; Transonic) was inserted in the right carotid artery and carefully pushed forward into the LV. The catheter's position inside the ventricle was optimized until rectangle-shaped loops were obtained. PV loops were conducted under short-time apnea. During the PV loop measurements, inferior vena cava was occluded by gentle compression. To estimate the volume, a bolus of hypertonic saline (10%) was injected into the left jugular vein.[29] Data were acquired using iox2 (Emka Technologies). Heart rate, maximum rate of LV pressure development in systole (dP/dtmax), maximal rate of LV pressure development in diastole (dP/dtmin), LV end-diastolic volume (LVEDV), and LV end-systolic pressure (LVEDP) were measured. Some measurements were technically not sufficient in a few mice (2 WT-Empty and 2 KI-Empty mice) and were excluded for the global analysis, giving rise to 9 WT-Empty, 9 KI-Empty, and 11 KI-TTL mice for the analysis. Subsequent analyses of PV loops were performed in LabChart 7.3Pro (AD Instruments). For baseline analysis, 5 to 10 consecutive loops during end-expiratory ventilation pause were selected to calculate preload-dependent parameters. Preload-independent parameters were analyzed by selecting loops during inferior vena cava occlusion.[29] Four mice per group were excluded from the PV-loop analysis for insufficient occlusion. All included mice underwent appropriate levels of anesthesia and did not experience excessive bleeding during the procedure.

Protein Extraction and Western Blot Analysis

For experiments performed in neonatal and adult mice, Western blot of whole-heart (crude) protein extraction was performed to quantify TTL (1:500; Proteintech; 13618-1-AP), α-tubulin (1:1000, clone DM1A; Cell Signaling; 3873), detyrosinated tubulin (dTyr-tub; 1:1000; Abcam; ab48389), and dsRed (1:500; Takara Clontech; 632392) protein levels as described previously.[9] For experiments performed in 15-week-old WT and KI mice, cardiac soluble (cytosolic) and insoluble (SDS, 5%) proteins were sequentially extracted, as described previously.[16,17] For experiments performed in hiPSC-derived cardiomyocytes or EHTs, we used crude protein extracts. Proteins were separated on 12% SDS-polyacrylamide (29:1) or 4% to 15% precast polyacrylamide mini-gels (Bio-Rad; 4561086) and electrotransferred on nitrocellulose membranes. Primary antibodies were directed against the dTyr-tub and α-tubulin (1:2000 and 1:5000, both kindly provided by Marie-Jo Moutin, Grenoble, France),[30] α-tubulin (1:1000; Cell Signaling; 3873), dTyr-tub (1:1000; Abcam; ab48389), H3 (histone H3; 1:3000; Abcam; ab24834), or GAPDH (1:10 000; HyTest; 5G4). Specificity of the antibodies was previously reported for α-tubulin and the 2 dTyr-tub antibodies.[9,30] Secondary antibodies were peroxidase-conjugated anti-mouse (Jackson ImmunoResearch; 515-035-003; 1:10 000; Sigma; A90244), anti-rat (1:10 000; Jackson ImmunoResearch; 112-035-003), or anti-rabbit (1:6000; Sigma; A0545). Proteins were visualized with Clarity Western ECL substrate (Bio-Rad; 1705061), and signals were detected with the ChemiGenius² Bio Imaging System (Bio-Rad).

Titin Isoform Analysis on Mouse Cardiac Crude Protein Fractions

Titin isoforms were separated on a 1% w/v agarose gel and stained with the SYPRO Ruby protein gel stain (Thermo Fisher Scientific; S12000) as described previously.[31] All samples were measured in triplicate and the average of triplicate measurements per sample was shown.

Immunofluorescence Analysis of hiPSC Cardiomyocytes

Two-dimensional culture of cardiomyocytes from the 3 hiPSC lines was seeded onto black, Geltrex-coated 96-well plates (Thermo Fisher Scientific; 165305) with 90 000 cells/cm² and cultured in low glucose DMEM-based medium for 30 days until cells were washed with PBS and fixed with ROTIHistofix (Carl Roth, P087.1) for 10 minutes at 4 °C. For immunofluorescence imaging, cells were incubated with blocking buffer (PBS containing 3% milk and 0.1% Triton X-100) and primary antibodies against mouse ACTN2 (α-actinin-2; 1:800; Sigma; A7811), rabbit dTyr-tub (1:1000, kindly provided by Marie-Jo Moutin, Grenoble, France), and mouse N-cadherin (1:500; Sigma; C2542) overnight. Specificity of the antibodies was previously reported for ACTN2,[25] dTyr-tub[30] and for N-cadherin.[32] Cells were washed with PBS and incubated with secondary antibodies AF-488 rabbit and AF-647 mouse (1:800; Thermo Fisher Scientific; A-11034 and A-21236) in blocking buffer for 90 minutes at room temperature. Hoechst 33342 (Invitrogen; H3570) was added 1:2500 for 20 minutes to stain DNA. Image acquisition was performed with a Zeiss LSM 800 confocal microscope.

RNA Sequencing

For RNA-seq, total RNA was isolated from LV samples of female WT-Empty, KI-Empty, and KI-TTL mice or from WT, SVBP-KO, and TTL-KO EHTs using the Direct-zol RNA Microprep Kit (Zymo Research; R2063) followed by a DNase digestion step. Enrichment of mRNAs with the NEBNext Poly(A) mRNA Magnetic Isolation Module was followed by library preparation using the NEBNext Ultra II RNA Directional Library Prep Kit for Illumina (New England BioLabs; E7760L). Single-read sequencing took place on the NextSeq 2000 System (Illumina), using the corresponding NextSeq 2000 P3 Reagents (50 cycles), with a read length of 72 base pairs. The integrity of the RNA and quality of the library were assessed using TapeStation 4200 (Agilent).

The sequencing data were automatically demultiplexed using the Illumina BCL Convert Software v3.8.2. FastQ files underwent pretrimming and postalignment quality control rounds using FastQC v0.11.7 (https://www.bioinformatics.babraham.ac.uk/projects/fastqc/). Removal of Illumina adapters and low-quality sequences was performed with Trimmomatic v0.38.[33] Reads of length <15 bases, as well as leading and trailing bases with quality <3 or no base call, and bases with average quality <15 in a 4-base sliding window were removed. Alignment was performed with HISAT2 v2.1,[34] using the mouse genome assembly mm10 (*Mus musculus*, GRCm38) or the human reference genome GRCh38, version 90. Mapped reads (primary alignments) were sorted by read name using SAMtools v1.8,[35] and read counts were calculated with HTSeq v0.11.2.[36]

Differential expression was assessed using the software package DESeq2[37] for all possible comparisons. Raw read counts were filtered to remove genes with <10 counts before analysis. Here, statistical significance of coefficients was tested using a negative binomial generalized linear model with the Wald test, and *P* values were adjusted for multiple comparisons following the Benjamini-Hochberg method (P_{adj}). Genes were considered differentially expressed at P_{adj} values <0.05.

To provide a biological context, each list of differentially expressed genes was subjected to functional enrichment analysis using the web tool g:GOSt from g:Profiler.[38] All gene ontology (GO) and pathways gene set categories available for Mus musculus or Homo sapiens within this tool were retrieved. Gene sets were considered significantly enriched following a hypergeometric test for overrepresentation within annotated genes, corrected for multiple comparisons using the Benjamini-Hochberg method (P_{adj}<0.05).

NanoString RNA Analysis

Total RNA was extracted from powdered whole-heart tissue samples using the SV Total RNA Isolation kit (Promega, Madison, WI; Z3105) according to the manufacturer's instructions or from hiPSC-derived cardiomyocyte extracts with the TRIzol reagent (Invitrogen; 15596018). RNA concentration, purity, and quality were determined using the NanoDrop ND-1000 spectrophotometer (Thermo Fisher Scientific). For gene expression analysis, customized NanoString nCounter Elements TagSet panels were used (Table S1). About 50 ng RNA of each sample was hybridized to the target-specific capture and reporter probes at 67 °C overnight (16 hours) according to the manufacturer's instructions. Samples were cooled down to 4 °C, supplemented with 15 µL H_2O, and loaded into the NanoString cartridge. Afterward, the nCounter Gene Expression Assay was started immediately. Raw data were analyzed with the nCounter Sprint Profiler. Transcript levels were determined with the nSolver Data Analysis Software including background subtraction using negative controls and normalization to 6 housekeeping genes (*Abcf1*, *Actb*, *Cltc*, *Gapdh*, *Pgk1*, and *Tubb5*).

MS-Based Proteomics

Mouse LV and EHT samples were dissolved in 100 mmol/L triethyl ammonium bicarbonate (Thermo Fisher Scientific; 90114) and 1% w/v sodium deoxycholate (Sigma-Aldrich; 30970) buffer, boiled at 95 °C for 5 minutes, and sonicated with a probe sonicator. The protein concentration of denatured proteins was determined by the Pierce bicinchoninic acid assay (Thermo Fisher Scientific; 23227).

Mouse samples were diluted to 20 µg protein in 25 µL buffer. The samples were then pipetted into a 96-well LoBind plate (Eppendorf SE; 003012951) placed on Andrew+ Pipetting Robot (Waters; 720007789EN), which was used to execute all following steps. Using the robot, disulfide bonds were first reduced in 10 mmol/L dithiothreitol (Roche; 11583786001) for 30 minutes at 56 °C while shaking at 800 rpm and alkylated in the presence of 20 mmol/L iodoacetamide (Sigma-Aldrich; J6125) for 30 minutes at 37 °C, again while shaking at 800 rpm. Then, carboxylate-modified magnetic E3 and E7 speed beads (Cytvia Sera-Mag, 65152105050250 and 45152105050250) at 1:1 ratio in liquid chromatography with tandem mass spectrometry (LC-MS/MS) grade water (Chemsolute, 455.1000) were added in a 10:1 (beads per protein) ratio to each sample, following the single-pot, solid-phase enhanced sample preparation (SP3) protocol workflow.[39] To bind the proteins to the beads, acetonitrile (ACN; Chemsolute, 2653.1000) concentration was raised to 50%. Subsequently, samples were shaken at 600 rpm for 18 minutes at room temperature. Magnetic beads were magnetized, and the supernatant was removed. Magnetic beads were further washed 2× with 80% ethanol (Supelco; 1.11727.1000) and then 2× with 100% ACN. After resuspension in 100 mmol/L AmBiCa (Sigma-Aldrich; 09830), digestion with trypsin was performed (sequencing grade modified trypsin; Promega; V5111) at 1:100 (enzyme:protein) ratio at 37 °C overnight while shaking at 500 rpm. The next day, trifluoroacetic acid (Sigma-Aldrich; 80457) was added to a final concentration of 1% to inactivate trypsin. The samples were then shaken at 500 rpm for 5 minutes at room temperature. Finally, beads were magnetized, and the supernatant containing tryptic peptides was transferred into a new 96-well LoBind plate, ready for subsequent LC-MS/MS analysis. For LC-MS/MS data acquisition, chromatographic separation of 1 µL tryptic peptides was achieved with a 2-buffer system (buffer A: 0.1% formic acid [FA; Fisher Chemical; A117-50] in H_2O, buffer B: 0.1% FA in ACN) on Ultra High Performance Liquid Chromatography (UHPLC; Vanquish Neo UHPLC system; Thermo Fisher Scientific; VN-S10-A-01). Attached to the UHPLC was a peptide trap (300 µm×5 mm, C18, PepMap Neo Trap Cartridge; Thermo Fisher Scientific; 174500) for online desalting and purification, followed by a 25-cm C18 reversed-phase column (75 µm×250 mm, 130 Å pore size, 1.7 µm particle size, peptide BEH C18, nanoEase; Waters; 186008795). Peptides were separated using an 80-minute method with linearly increasing ACN concentration from 2% to 30% ACN over 60 minutes. MS/MS measurements were performed on a quadrupole-orbitrap hybrid mass spectrometer (Exploris 480; Thermo Fisher Scientific; BRE725533). Eluting peptides were ionized using a nano-electrospray ionization source with a spray voltage of 1800 and analyzed in data-dependent acquisition mode. For each MS1 scan, ions were accumulated for a maximum of 25 ms or until a charge density of 1×106 ions (automatic gain control [AGC] target) was reached. Fourier transformation−based mass analysis of the data from the orbitrap mass analyzer was performed covering a mass range of m/z 350 to 1400 with a resolution of 60 000 at m/z 200. Peptides being responsible for the 20 highest signal intensities per precursor scan with a minimum AGC target of 8×103 and charge state from +2 to +6 were

isolated within an m/z 2 isolation window and fragmented with a normalized collision energy of 30% using higher energy collisional dissociation. MS2 scanning was performed, covering a mass range starting at m/z 120 and accumulated for 50 ms or to an AGC target of 1×105 at a resolution of 15 000 at m/z 200. Already fragmented peptides were excluded for 30 s.

For proteome analysis of EHTs, 20 µg of protein of each sample was taken and disulfide bonds reduced in the presence of 10 mmol/L dithiothreitol at 60 °C for 30 minutes. Cysteine residues were alkylated in the presence of 20 mmol/L iodoacetamide at 37 °C in the dark for 30 minutes, and tryptic digestion (sequencing grade; Promega; V5111) was performed at a 100:1 protein to enzyme ratio at 37 °C overnight. Digestion was stopped and sodium deoxycholate precipitated by the addition of 1% v/v FA. Samples were centrifuged at 16 000g for 5 minutes, and the supernatant was transferred into a new tube. Samples were dried in a vacuum centrifuge. Samples were resuspended in 0.1% FA and transferred into a full recovery autosampler vial (Waters). Chromatographic separation was achieved on a nano-UPLC system (Dionex Ultimate 3000 UPLC system; Thermo Fisher Scientific; IQLAAAGABHFAPBMBEY) with a 2-buffer system (buffer A: 0.1% FA in water, buffer B: 0.1% FA in ACN). Attached to the UPLC was a reversed-phase trapping column (Acclaim PepMap 100 C18 trap, 100 µm×2 cm, 100 Å pore size, 5 µm particle size; Thermo Fisher; 164750) for desalting. Purification was followed by a reversed-phase capillary column (nanoEase M/Z peptide BEH130 C18 column, 75 µm×25 cm, 130 Å pore size, 1.7-µm particle size; Waters). Peptides were separated using a 60-minute gradient with increasing ACN concentration from 2% to 30%. The eluting peptides were analyzed on a quadrupole-orbitrap ion trap tribrid mass spectrometer (QExactive; Thermo Fisher Scientific; IQLAAEGAAPFALGMAZR) in data-dependent acquisition mode. For data-dependent acquisition analysis, the fusion was operated at top speed mode analyzing the most intense ions per precursor scan (2×105 ions, 120 000 resolution, 120-ms fill time) within 3 s and were analyzed by MS/MS in the ion trap (higher energy collisional dissociation at 30 normalized collision energy, 1×104 ions, 60-ms fill time) in a range of 400 to 1300 m/z. A dynamic precursor exclusion of 20 s was used.

LC-MS/MS data were searched with the Sequest algorithm integrated into the Proteome Discoverer software (mouse LV: v3.1.0.638; EHTs: v2.4.1.15; Thermo Fisher Scientific) against a reviewed Swissprot database. Carbamidomethylation was set as a fixed modification for cysteine residues. The oxidation of methionine, as well as acetylation of the protein N terminus and methionine loss were allowed as variable modifications. A maximum number of 2 missing tryptic cleavages was set. Peptides between 6 and 144 amino acids were considered. A strict cutoff (false discovery rate [FDR]<0.01) was set for peptide and protein identification. Quantification was performed using the Minora algorithm, implemented in Proteome Discoverer. Obtained protein abundances were log2-transformed and normalized by column-median normalization. Further statistical testing was performed in Perseus (Maxquant; Max Planck Institute of Biochemistry).[40] Student t test was applied including FDR correction (q values) of obtained P values based on the Benjamini-Hochberg method.

Presentation of Omics Data

For RNA-seq, nanostring, and MS analyses, data are expressed as log2 ratio, which represents the difference in log2 mean value between the test and reference groups (=log2[test]−log2[reference]) where the mean of log2(reference) was set to 0. Dot plots were created with the clusterProfiler R package in Rstudio, version 2023.12.1,[41] with adjusted P values (P_{adj}) obtained with the Benjamini-Hochberg method for multiple comparisons.

Statistical Analysis

The precise number of samples (N), females (F), males (M), technical replicates (n), biological replicates (d), and outliers is indicated in the figure legends. Statistical analyses were performed with GraphPad Prism8 (GraphPad Software, Inc, Boston, MA), and data are expressed as mean±SEM. Data were assessed for normality with the Shapiro-Wilk test. For the data that did not pass this test, we applied the Kolmogorov-Smirnov test. In cases where normal distributions were not met with both tests, we did a robust regression and outlier removal (ROUT) analysis at 1% to detect potential outliers that were removed from the analysis. Then, when normal distributions were not met or when the sample size was insufficient to test normality (eg, n<6), a nonparametric test was applied.

Statistical significance for 2-group comparison was performed with the unpaired Student t test. Multiple group comparison was performed with 1-way ANOVA and Dunnett multiple comparisons test or with the nonparametric Kruskal-Wallis test and Dunn multiple comparisons test. When no equal SDs were assumed, we used the Brown-Forsythe and Welch ANOVA test and Dunnett T3 multiple comparisons test. Two-way multiple group comparison was performed by fitting a mixed-effects model with the Geisser-Greenhouse correction and Dunnett multiple comparisons test. All multiple comparison tests were performed only within each analysis. Statistical tests are indicated in the figure legends. The precise P values are written in scientific notation, and a P value <0.05 was considered statistically significant.

RESULTS

Long-Term TTL Overexpression Leads to a Dose-Dependent Reduction in Myocyte Stiffness and Improves Contractility in Rodent Ventricular Myocytes

We first evaluated the effect of TTL overexpression on reducing myocardial dTyr-tub level in healthy C57/BL6J mice. For the initial study, we tested 2 different doses of AAV9 (1.75E11 and 9E11 vg/g) encoding TTL-dsRed driven under the *TNNT2* promoter (Figure S1A). Mice were injected at postnatal day 2 (P2), and after 6 weeks of expression, the myocardial tissue was harvested (Figure 1A). As expected, TTL levels increased in the myocardium in a dose-dependent manner, which was concomitant with decreased dTyr-tub level (Figure 1B). A strong inverse correlation was observed across myocardial samples between increased dsRed and reduced dTyr-tub levels, suggesting that dsRed can be utilized as a useful indicator of the dTyr-tub level (Figure 1C). To evaluate transduction
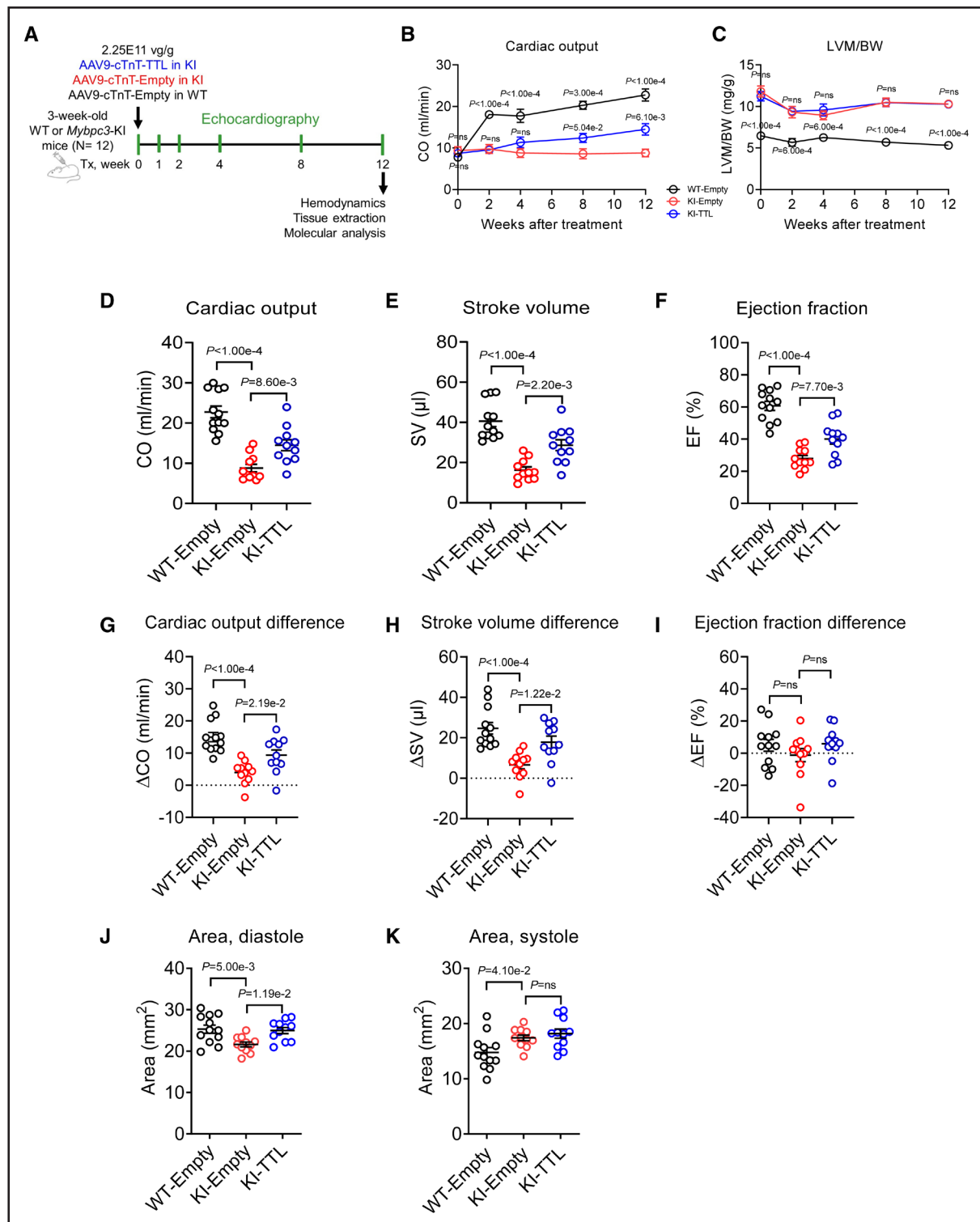
Figure 2. Evaluation of the cardiac phenotype by echocardiography after AAV9-TTL/-Empty treatment.
A, Protocol: 3-week-old wild-type (WT) and *Mybpc3*-targeted knock-in (KI) mice were included in the study. Mice received a dose of 2.25E11 vg/g of either AAV9-Empty (no insert) or AAV9-TTL (hemagglutinin [HA]-tagged human TTL) under the control of human cTnT (TNNT2 [tropinin T2, cardiac type]) promoter for 12 weeks. **B**, Cardiac output (CO) over time. **C**, Left ventricular mass (LVM)/body weight (BW) ratio over time. Evaluation after 12 weeks of (**D**) CO, (**E**) Stroke volume (SV) and (**F**) Ejection fraction (EF). Difference in value per mouse between the last and basal echocardiography for (**G**) CO (ΔCO), (**H**) SV (ΔSV), and (**I**) EF (ΔEF). **J**, Left ventricular area in end diastole after 12 weeks. **K**, Left ventricular area in end systole after 12 weeks. Data are expressed as mean±SEM. Statistical significance was assessed vs KI-Empty by fitting a mixed-effect model with the Geisser-Greenhouse correction (**B** and **C**) or by 1-way ANOVA (**D–K**), followed by Dunnett multiple comparisons test, with N/F/M=12/7/5 (WT-Empty) and N/F/M=12/10/2 (KI-Empty). AAV9 indicates adeno-associated virus serotype 9; N/F/M, number of mice/female/male; TTL, tubulin tyrosine ligase; and Tx, treatment.
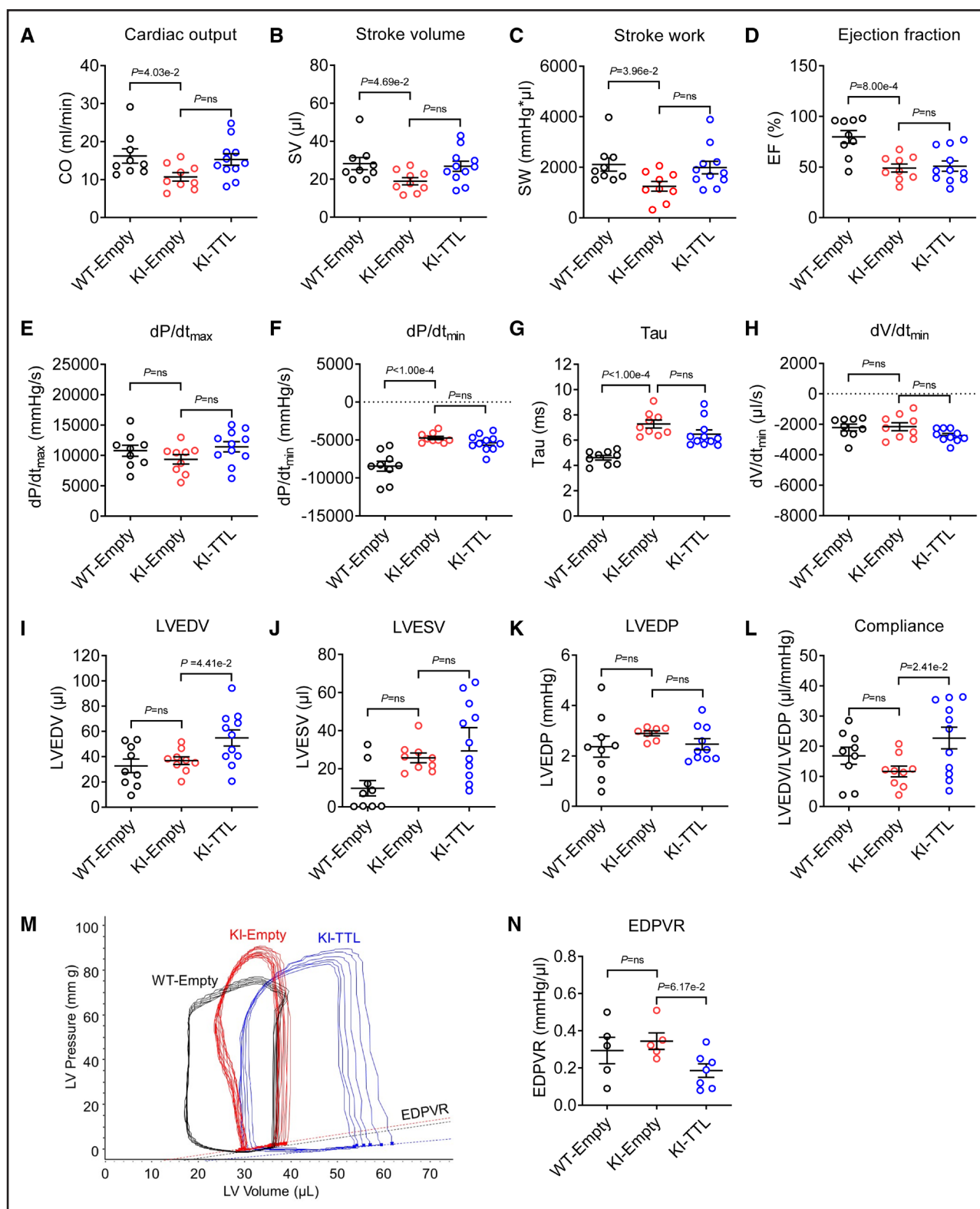
Figure 3. Evaluation of the cardiac phenotype by hemodynamics after a 12-week AAV9-TTL/-Empty treatment.

Three-week-old wild-type (WT) and *Mybpc3*-targeted knock-in (KI) mice received either AAV9-Empty (no insert) or AAV9-TTL (HA-tagged human TTL). Global function is represented by (**A**) cardiac output (CO), (**B**) stroke volume (SV), and (**C**) stroke work (SW). Contractility is represented by (**D**) ejection fraction (EF) and (**E**) maximum rate of left ventricular (LV) pressure change (dP/dt$_{max}$). Relaxation is represented by (**F**) minimal rate of LV pressure change (dP/dt$_{min}$) and (**G**) time constant of active relaxation (τ), calculated with the Weiss method. LV filling is represented by (**H**) minimal rate of LV volume change (dV/dt$_{min}$), (**I**) LV end-diastolic volume (LVEDV), and (**J**) LV end-systolic volume (LVESV). Stiffness is represented by (**K**) LV end-diastolic pressure (LVEDP) and (**L**) compliance. **M**, Pressure/volume (PV) loop traced after increasing occlusion (*Continued*)

efficiency, we isolated cardiomyocytes 6 weeks after a single intermediate dose of AAV9-TTL-dsRed (4.4E11 vg/g) and binned them based on their dsRed fluorescence levels relative to a noninjected control. We found that 85% of myocytes from the injected hearts exhibited dsRed levels above that of noninjected controls, with heterogenous levels of expression between transduced myocytes (Figure 1D). As a second proof-of-concept study, we administered AAV9-TTL-dsRed (5.625E11 vg/g) in 6-week-old mice and harvested myocardial tissue for Western blot 6 weeks later. Consistently, we saw a ≈15-fold accumulation of TTL and a robust reduction in dTyr-tub with no change in total α-tubulin levels (Figure S1C and S1D).

We next evaluated isolated cardiomyocyte function upon TTL overexpression. We injected a single intermediate dose of AAV9-TTL-dsRed into P4 rats (4.4E11 vg/g) and isolated single cardiomyocytes 6 weeks later (Figure 1E). Rat myocytes were used for their robustness for functional characterization in our hands.[8,9] We took advantage of the heterogeneous expression of TTL-dsRed between cardiomyocytes from a given heart to compare myocyte properties to nonexpressing controls from the same animal. Myocytes from transduced hearts could be binned into tertiles based on their TTL level (measured by dsRed intensity): (1) those expressing no/low levels of TTL (dsRed intensity within the range of uninjected myocytes, 52%), (2) those with moderate TTL expression (10−20× increase in the dsRed level compared with control mean, 23%), and (3) those with high TTL overexpression (>20× increase in the dsRed level, 27%).

Myocytes were assessed for changes in myocyte stiffness, intracellular calcium dynamics, and unloaded shortening upon TTL overexpression. Following the functional assessment (blind to expression level), myocytes were binned into TTL expression tertiles. Myocytes expressing TTL showed a dose-dependent reduction in myocyte viscoelasticity as measured via transverse nanoindentation (Figure 1F). Consistent with reduced internal stiffness, myocytes showed a TTL dose-dependent increase in fractional shortening and contractile kinetics (Figure 1G), which appeared to be independent of any changes in intracellular calcium cycling (Figure 1H). These data reflect previous observations obtained in human failing and nonfailing cardiomyocytes after acute (48 hours) adenovirus-mediated TTL overexpression[9] and suggest that the rapid reduction in myocyte stiffness and improved contractility (independent of calcium

transient alterations as previously shown[8]) persist with chronic TTL overexpression.

Chronic TTL Overerzxpression Improves Cardiac Function in *MYBPC3*-Targeted KI Mice

Next, we evaluated whether chronic TTL application could rescue the cardiac disease phenotype of the HCM KI mice in vivo. KI mice developed LV hypertrophy combined with systolic and diastolic dysfunction.[10,11] The AAV9-Empty or AAV9-TTL vector was systemically delivered with a dose of 2.25E11 vg/g in 3-week-old WT and KI mice (Figure 2A; Figure S1F). Cardiac function was evaluated by serial echocardiography at baseline and 1, 2, 4, 8, and 12 weeks after treatment (Figure 2A; Table S2). CO was lower and LV mass/BW ratio was higher in KI-Empty mice compared with WT-Empty mice over the course of the experiment (Figure 2B and 2C). Chronic TTL overexpression significantly improved CO overtime but not LV mass/BW in KI mice (Figure 2B and 2C). After 12 weeks, CO, SV, and ejection fraction (EF) were lower in KI-Empty than in WT-Empty mice, and TTL partially ameliorated these parameters in KI mice (Figure 2D through 2F). When evaluating the change in global function within an individual animal from the first-to-last echocardiography, TTL significantly increased CO and SV, but not EF, compared with KI-Empty mice (Figure 2G through 2I). Finally, TTL overexpression increased LV area at end diastole, but not at end systole, in KI mice (Figure 2J and 2K). Similar functional and morphological changes were also present when only female mice were considered (Figure S3). These data suggest that TTL improves global heart function independent of robustly increasing contractility in KI mice.

At the end of the 12-week treatment, mice were subjected to hemodynamic measurements by LV catheterization (Figure 3; Table S3). In accordance with the echo findings, global function (CO, SV, and stroke work) was lower in KI-Empty than in WT-Empty mice (Figure 3A through 3C). Systolic function (EF but not dP/dt_{max}) was lower in KI-Empty than in WT-Empty mice (Figure 3D and 3E). Diastolic relaxation (dP/dt_{min} and τ) was impaired (Figure 3F and 3G), whereas diastolic filling (dV/dt_{min}, LVEDV) did not differ to WT-Empty in KI-Empty mice (Figure 3H and 3I). Consistent with echo-derived area measurements, LV end-systolic volume was greater in KI-Empty than in WT-Empty mice (Figure 3J). Chronic TTL overexpression partially improved global function

Figure 3 Continued. in a representative mouse of each performed group. **N**, End-diastolic pressure-volume relation (EDPVR) calculated with a linear fit. Data are expressed as mean±SEM. Statistical significance was assessed in **A** through **L** with 1-way ANOVA and Dunnett multiple comparisons test (**A–L**), with N/F/M=9/5/4 (WT-Empty), 9/7/2 (KI-Empty), and 11/6/5 (KI-TTL); to pass the normality test, some outliers (robust regression and outlier removal [ROUT] 1%) were removed: 1 KI-TTL (**H**), 2 KI-Empty, and 1 KI-TTL (**K**). Statistical significance was assessed in **N** with Kruskal-Wallis test and Dunn multiple comparisons test with N/F/M=5/3/2 (WT-Empty), 5/4/1 (KI-Empty), and 7/3/4 (KI-TTL). ns, P>0.05. AAV9 indicates adeno-associated virus serotype 9; HA, hemagglutinin; N/F/M, number of mice/female/male; and TTL, tubulin tyrosine ligase.
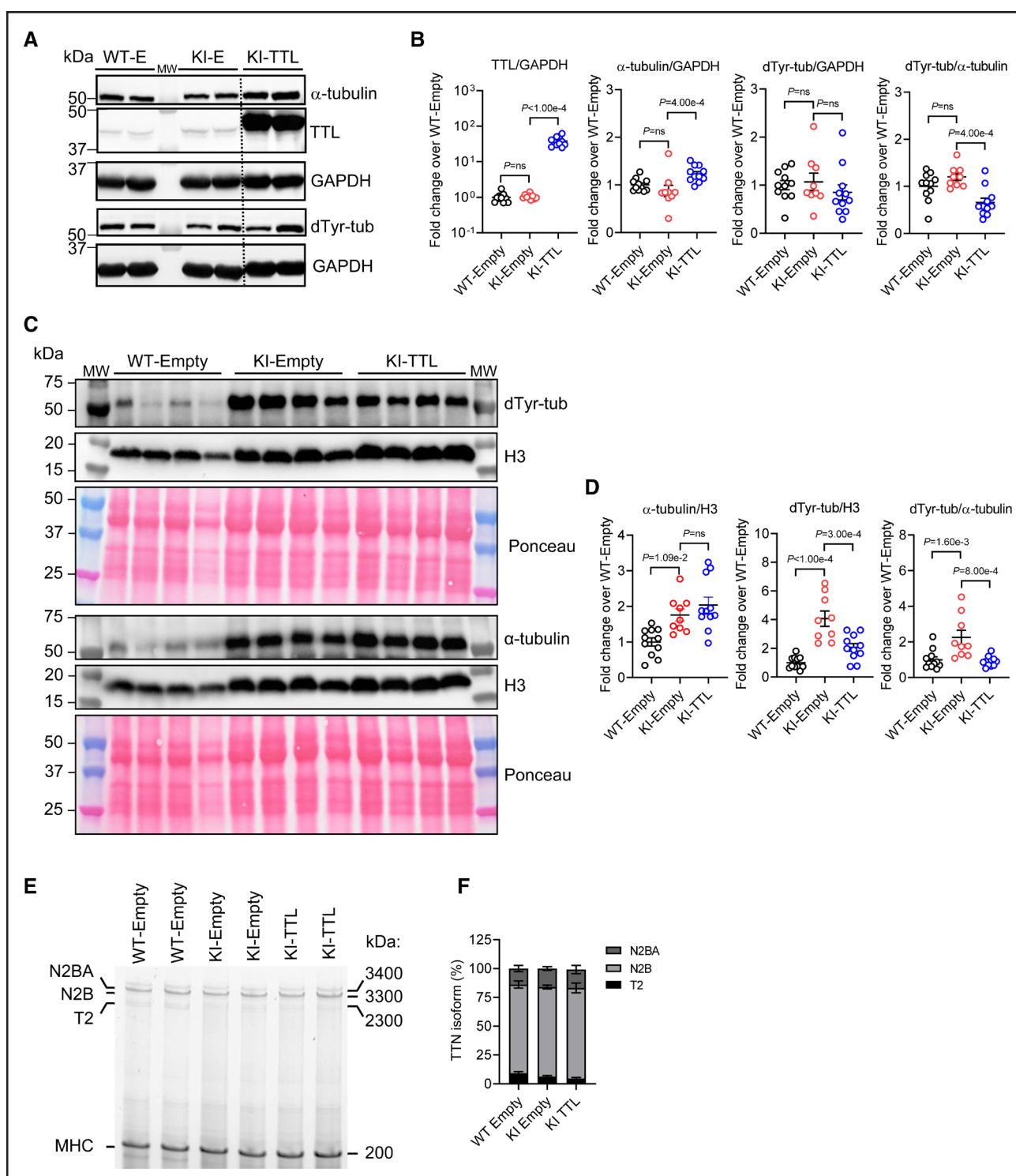
Figure 4. Molecular evaluation of tubulin detyrosination and titin isoforms in mice.
A, Representative Western blot of cardiac soluble (cytosolic) proteins stained for α-tubulin, TTL (tubulin tyrosine ligase), detyrosinated tubulin (dTyr-tub), and GAPDH as a loading control in WT-Empty (WT-E), KI-Empty (KI-E), and KI-TTL mice; dashed line indicates where the blots were cut. **B**, Protein levels of TTL/GAPDH, α-tubulin/GAPDH, dTyr-tub/GAPDH, and dTyr-tub/α-tubulin in WT-Empty (N/F/M=11/7/4), KI-Empty (N/F/M=9/8/1), and KI-TTL (N/F/M=11/6/5). **C**, Representative Western blot of cardiac insoluble proteins (SDS extracted) stained for dTyr-tub, α-tubulin, and H3 (histone H3) as a loading control, and the respective Ponceau staining. **D**, Protein levels of α-tubulin/H3, dTyr-tub/H3, and dTyr-tub/α-tubulin in WT-Empty (N/F/M=11/7/4), KI-Empty (N/F/M=9/8/1), and KI-TTL (N/F/M=11/6/5) samples. **E**, Representative SYPRO Ruby–stained agarose gel of cardiac crude protein fractions showing titin (isoforms N2BA, N2B, and T2) and myosin heavy chain (MHC). **F**, Percentage of N2BA, N2B, and T2 isoforms normalized to MHC, with N=5, 8, and 8 in WT-Empty, KI-Empty, and KI-TTL, respectively. Data are expressed as mean±SEM and relative to the mean of WT-Empty. Statistical significance vs KI-Empty was assessed with 1-way ANOVA and Dunnett multiple comparisons test. Two KI-Empty samples were removed for the quantification (**B** and **D**) because the insoluble proteins were degraded. ns, $P>0.05$. KI indicates knock-in; MW, molecular weight; N/F/M, number of mice/female/male; and WT, wild type.
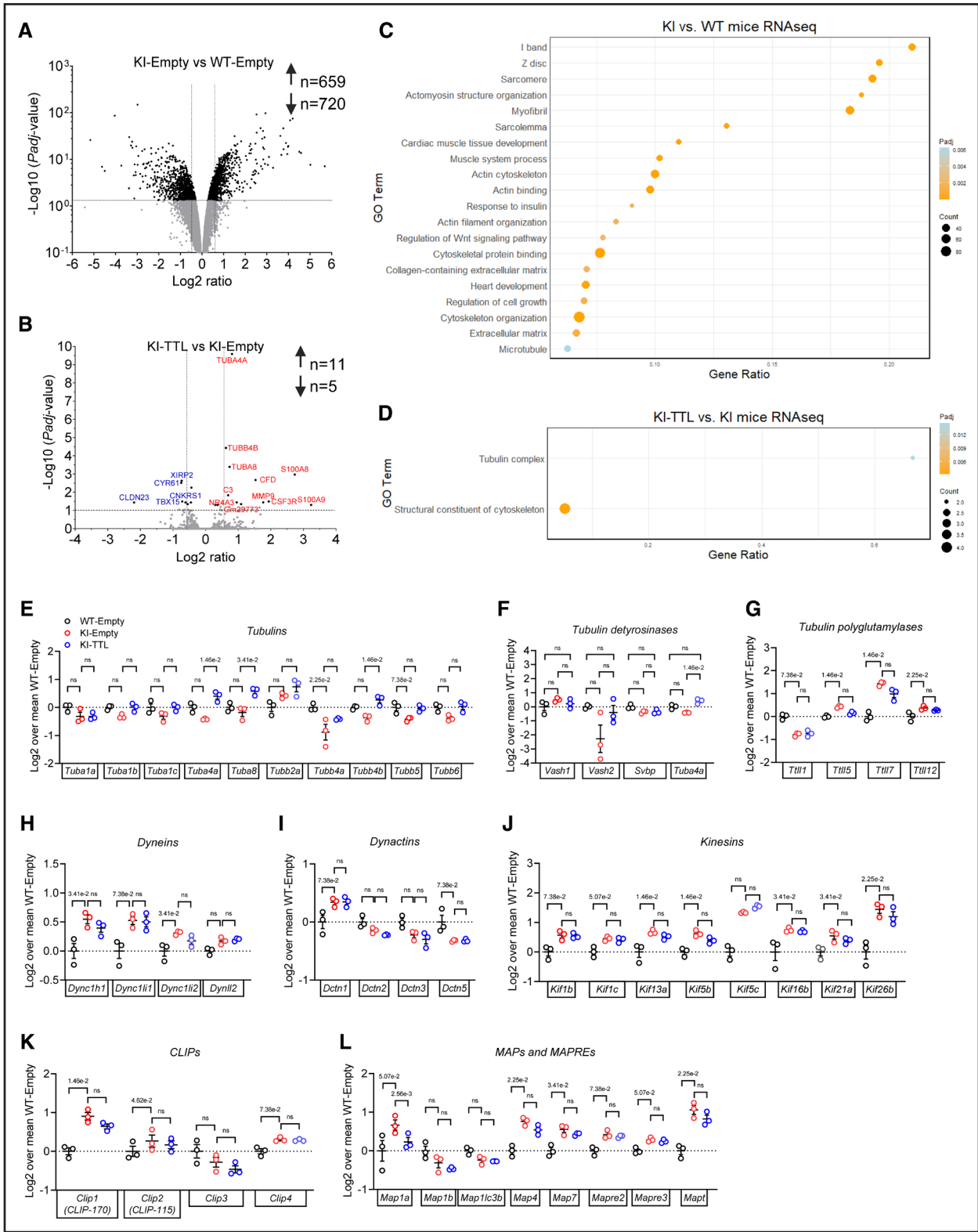
Figure 5. RNA-sequencing (RNA-seq) analysis in mouse hearts.
RNA-seq analysis was performed in female mouse LV tissue extracts (N=3). Volcano plots show the —log10 (P_{adj} value) vs the magnitude of change (log2 ratio=log2[case]—log2[reference]) of (**A**) mRNA levels in KI-Empty vs WT-Empty and (**B**) mRNA levels in KI-TTL vs KI-Empty. Light gray dots indicate P_{adj}>0.05, and black dots indicate P_{adj}<0.05. Dot plot of the gene ontology (GO) pathway enrichment map based on RNA-seq with significantly overrepresented pathways (P_{adj}<0.05) in (**C**) KI-Empty vs WT-Empty (log2 ratio, >0.58) and (**D**) KI-TTL vs KI-Empty (log2 ratio, >0.58 or <—0.58). The dot size is proportional to the number of gene counts, the *x* axis shows the gene ratio, and the heatmap color shows the extent of P_{adj} values from the lowest (orange) to the highest (blue). Specific mRNA levels of (**E**) tubulins, (**F**) tubulin detyrosinases, (**G**) tubulin polyglutamylases, (**H**) dyneins, (**I**) dynactins, (**J**) kinesins, (**K**) CLIPs (CAP-Gly domain-containing linker proteins), (*Continued*)

(CO, SV, and stroke work), though not significant with the 1-way ANOVA (Figure 3A through 3C). These parameters were significantly different when only KI-TTL and KI-Empty mice were compared (Table S3). Furthermore, whereas TTL overexpression did not improve systolic and diastolic relaxation parameters (Figure 3D through 3G), supporting echo data, it improved both the LV diastolic filling (Figure 3I) and LV compliance, determined by the LVEDV/LVEDP ratio (Figure 3L). PV loops of a representative mouse of each group at different stages of the occlusion showed higher LV pressure and lower SV in KI-Empty and a marked increase in LVEDV in the KI-TTL mouse, resulting in a higher SV (Figure 3B, 3J, and 3M). This was associated with a tendency to reduction in end-diastolic PV relation in KI-TTL (Figure 3N), suggesting reduced stiffness. Taken together, these data provide evidence that chronic TTL overexpression improved myocardial compliance and increased diastolic filling to restore CO in KI mice.

Chronic TTL Overexpression Reduces dTyr-MT Abundance in KI Mice

Cardiac proteins were extracted with a 2-step protocol giving rise to soluble (cytosolic) and insoluble (SDS extract) proteins. The levels of TTL, α-tubulin, dTyr-tub, and dTyr-tub/α-tubulin ratio, all normalized to GAPDH in the soluble fractions, did not differ between KI-Empty and WT-Empty mice (Figure 4A and 4B). Whereas TTL overexpression gave rise to a higher TTL level (37-fold) and α-tubulin level, it did not affect dTyr-tub level, resulting in a lower dTyr-tub/α-tubulin ratio in KI mice (Figure 4A and 4B). The increase in α-tubulin level was expected and inherent upon TTL expression, since tyrosination reduces microtubule stability and increases soluble tubulin.[9,42]

On the contrary, the levels of α-tubulin, dTyr-tub, and dTyr-tub/α-tubulin ratio, all normalized to H3 in the insoluble fraction, were higher in KI-Empty than in WT-Empty mice (Figure 4C and 4D). Increased level of α-tubulin is in agreement with our previous findings in KI crude protein fraction.[3] This suggests an increased, stable, dTyr-MT network in KI mice. TTL did not affect the level of α-tubulin, whereas it reduced the dTyr-tub level and fully normalized the dTyr-tub/α-tubulin ratio in KI mice. This indicates that TTL markedly reduced dTyr-MT in KI mice, in agreement with the data obtained in WT mice (Figure 1B; Figure S1B through S1D). The remaining dTyr-tub/H3 could be due to a compensatory role of other detyrosinases in KI mice such as TUBA4A (see below) and the recently discovered MATCAP1

(microtubule associated tyrosine carboxypeptidase 1)[43] in this process.

TTN Isoform Switch Is Not Involved in Decreased Stiffness in KI-TTL

We then evaluated whether the increased compliance/reduction in end-diastolic PV relation (Figure 3L and 3N) is the result of changes in titin isoform composition, leading to less N2B, stiff isoform, and more N2BA, compliant isoform, in KI-TTL. Long-run gel electrophoresis was performed as described previously[31] in the LV tissue extracted from the 3 mouse groups. No major difference was detected between the groups in the content of the 3 major isoforms of titin, N2BA, N2B and T2, and in the ratio of N2B/N2BA (Figure 4E and 4F). This suggests that titin isoform switch does not happen in KI mice and is not involved in the increased compliance/decreased stiffness in KI-TTL.

Chronic TTL Overexpression Induces Molecular Changes in KI Mice

To understand the molecular changes induced by long-term TTL overexpression, RNA-seq analyses were performed in female mouse LV tissue extracts. Gene expression analysis performed in 3 female samples per group revealed 1359 differentially expressed mRNAs (659 higher, 720 lower, log2 ratio >0.58 or <−0.58, P_{adj}<0.05) in KI-Empty than in WT-Empty mice and only 16 (11 higher, 5 lower, log2 ratio >0.58 or <−0.58, P_{adj}<0.05) in KI-TTL than in KI-Empty mice, including higher levels of several tubulin isoforms (Figure 5A and 5B). GO pathway analysis of RNA-seq data revealed enrichment (log2 ratio >0.58, P_{adj}<0.05) in components of the sarcomere, actin cytoskeleton, microtubule cytoskeleton, and extracellular matrix in KI-Empty versus WT-Empty mice (Figure 5C; Data Set S1). Since the number of significantly higher and lower mRNAs in KI-TTL versus KI-Empty mice was low, GO analysis was done on all (log2 ratio >0.58 or <−0.58, P_{adj}<0.05) and revealed the tubulin complex and structural components of the cytoskeleton as the only significantly dysregulated pathways (Figure 5D; Data Set S1).

We then compared the RNA-seq data for several components associated with the microtubule network with the Kruskal-Willis nonparametric test in the 3 groups. The data show a trend to lower mRNA levels of most tubulin alpha and beta isoforms (*Tuba1b*, *Tuba1c*, *Tuba4a*, *Tubb4b*, *Tubb5*, and *Tubb6*) in KI-Empty mice and a normalization with TTL treatment (Figure 5E).

Figure 5 Continued. (**L**) MAPs (microtubule-associated proteins), and microtubule-associated protein RP/EB family members (MAPREs). Data are expressed as log2±SEM over mean of WT-Empty. Statistical significance was assessed for each gene of interest vs KI-Empty with Kruskal-Wallis test and Dunn multiple comparisons. ns, *P*>0.08. KI indicates knock-in; LV, left ventricle; N, number of mice; TTL, tubulin tyrosine ligase; and WT, wild type.

Tuba4a, *Tubb2a*, and *Tuba8* mRNA levels were even higher in KI-TTL than in WT-Empty mice (Figure 5E). The mRNA levels of the main tubulin detyrosinases (*Vash1*, *Vash2*, and *SVBP*) did not differ between the groups, whereas *Tuba4a*, encoding a dTyr-tub isoform, exhibited a higher level in KI mice treated with TTL (Figure 5F). The mRNA levels of tubulin polyglutamylases were dysregulated in KI-Empty mice, and TTL almost completely normalized *Ttll5* that prefers α- over β-tubulins in KI mice (Figure 5G). Several mRNAs encoding other microtubule-associated components were altered in KI-Empty mice and were not affected by TTL overexpression, such as the molecular motors dyneins, dynactins, and kinesins (Figure 5H through 5J), CLIPs (CAP-Gly domain-containing linker proteins), MAPs (microtubule-associated proteins), and MAP RP/EB family members (Figure 5K and 5L). This suggests an abundant bidirectional transport phenotype in KI mice. These data were supported by the quantification of selected mRNAs using the nanoString nCounter Elements technology and customized mouse-specific panels (Table S1) on a larger sample size (N=6−9; Figure S4A and S4B). Several genes altered in heart failure were dysregulated

in KI-Empty mice, such as *Myh7*, *Rcan1*, *Nppb*, *Fhl1*, *Myh6*, *Col1a1*, *Postn*, *Fhl2*, *Pln*, and *Ppp1r1a* (Figure S4A). Similarly, the levels of mRNAs encoding proteins of the autophagy-lysosomal pathway such as *Bag3*, *Sqstm1*, *Jak1*, *Lamp1*, *Chmp2b*, and *Epg5* were higher in KI-Empty mice (Figure S4A), as shown previously.[44] The levels of mRNAs encoding MAPs, such as *MAPT*, *Clip1*, *Mapre3*, *KiF5b*, *Map4*, *Dync1h1*, *Hdac6*, *Map1lc3a*, and *Actr1a*, were higher in KI-Empty than in WT-Empty mice (Figure S4A). TTL partially reversed the pattern in KI mice with higher mRNA levels for several tubulin isoforms and a lower mRNA level for *Hdac6*, encoding the α-tubulin deacetylase (Figure S4B).

MS analyses were performed in insoluble and soluble protein LV extracts from all available mouse LV samples (N=11 WT-Empty, N=9 KI-Empty, and N=10 KI-TTL mice). Volcano plot from insoluble protein fractions revealed 89 and 30 proteins with higher and lower levels in KI-Empty versus WT mice, respectively (log2 ratio >0.58 or <−0.58, P_{adj}<0.05; Figure 6A; Data Set S2). Interestingly, the fast skeletal MYBPC2 (myosin-binding protein C2) compensated the low level of MYBPC3 in KI mice. GO pathway analysis revealed the cytoskeleton
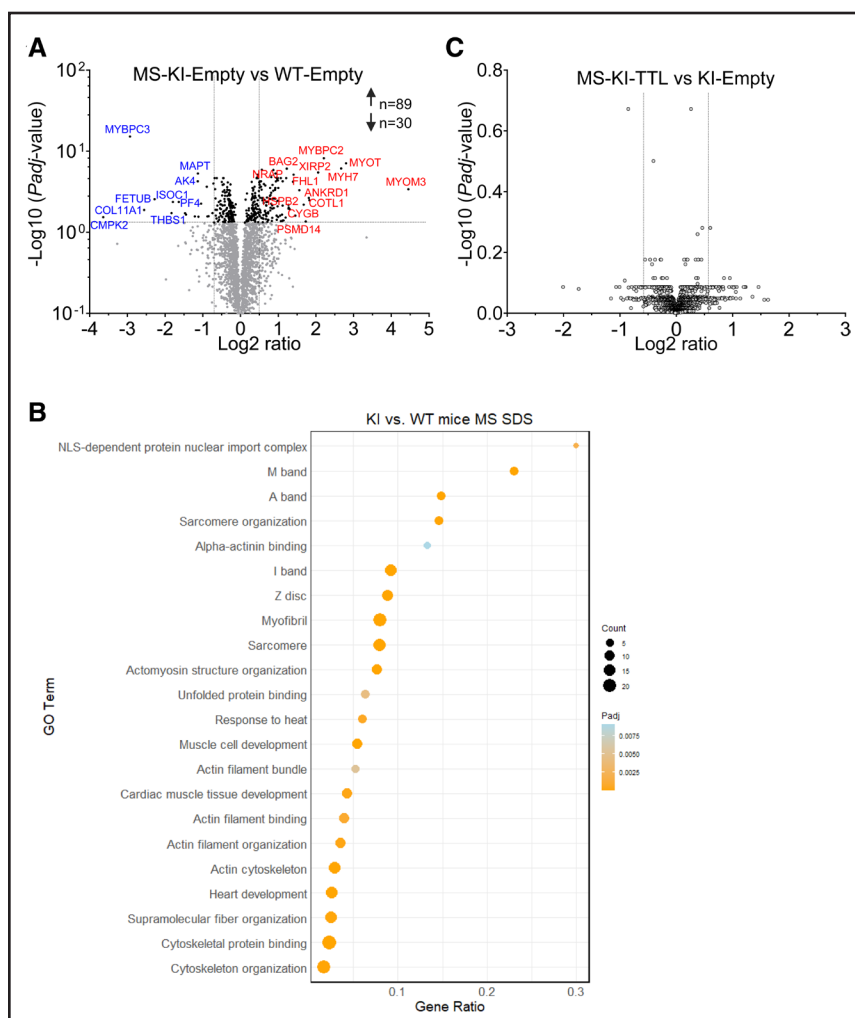

Figure 6. Proteomic analysis in mouse hearts.
Mass spectrometry (MS) analyses were performed in insoluble protein fraction from LV tissue of WT-Empty (N/F/M=11/7/4), KI-Empty (N/F/M=9/8/1), and KI-TTL (N/F/M=10/5/5). **A**, Volcano plots show the −log10 (P_{adj} value) vs the magnitude of change (log2 ratio=log2[case]−log2[reference]) of protein levels in KI-Empty vs WT-Empty. Light gray dots indicate P_{adj}>0.05, and black dots indicate P_{adj}<0.05. **B**, Dot plot of the gene ontology (GO) pathway enrichment map based on MS performed on insoluble LV protein fractions with significantly overrepresented pathways (P_{adj}<0.05) in KI-Empty vs WT-Empty (log2 ratio, >0.58). The dot size is proportional to the number of gene counts, the x axis shows the gene ratio, and the heatmap color shows the extent of P_{adj} values from the lowest (orange) to the highest (blue). **C**, Volcano plots show the −log10(P_{adj} value) vs log2 ratio of protein levels in KI-TTL vs KI-Empty. KI indicates knock-in; LV, left ventricle; N/F/M, number of mice/female/male; TTL, tubulin tyrosine ligase; and WT, wild type.
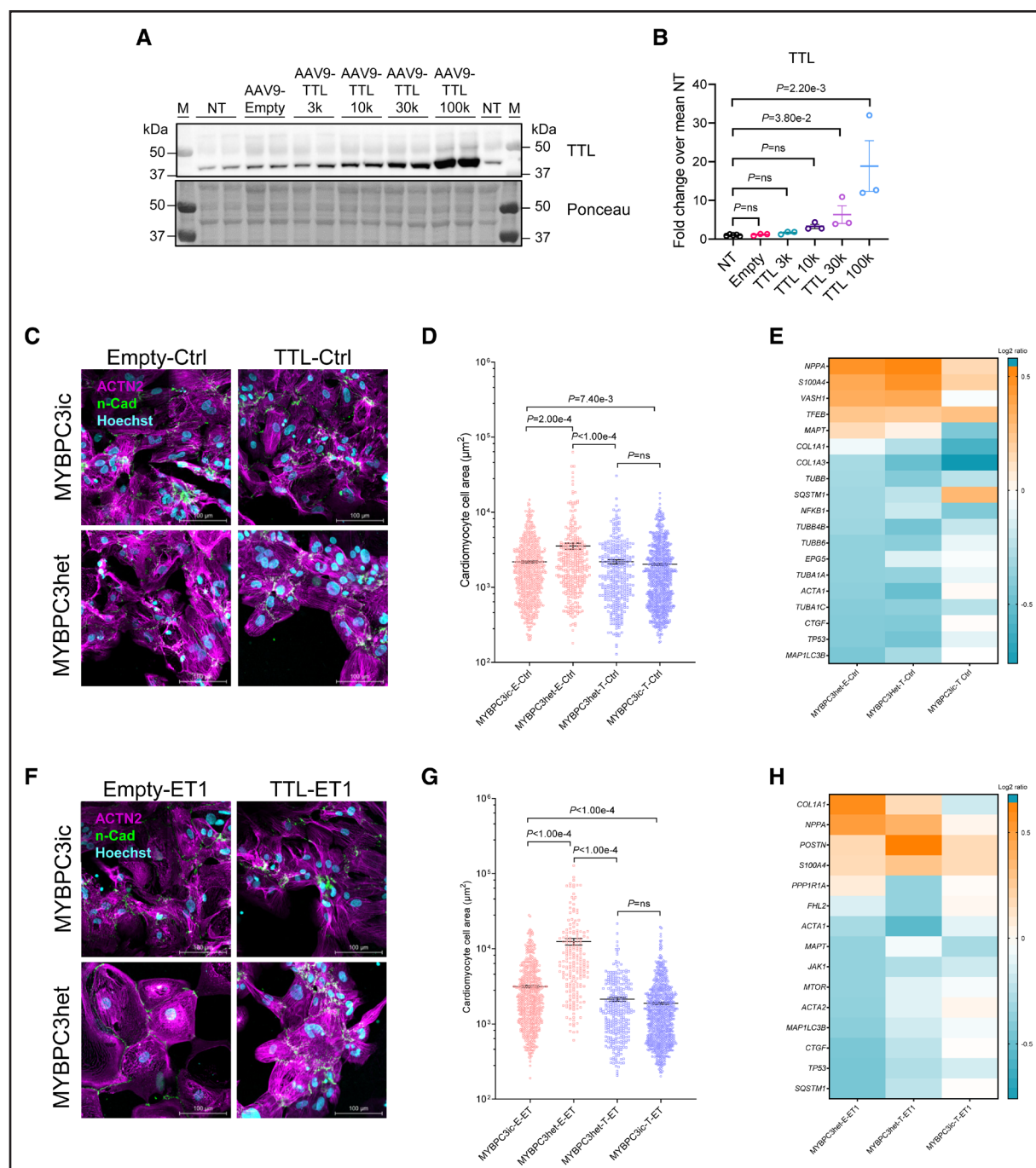
Figure 7. Evaluation of adeno-associated virus serotype 9 (AAV9)–mediated TTL (tubulin tyrosine ligase) transfer in MYBPC3 isogenic control (MYBPC3ic) and heterozygous MYBPC3 (MYBPC3het) human induced pluripotent stem cell (hiPSC)–derived cardiomyocytes.

MYBPC3ic hiPSC line was differentiated into cardiomyocytes for 2 weeks and then nontransduced (NT), transduced with AAV9-Empty (multiplicity of infection [MOI], 30 k), or transduced with AAV9-TTL (MOI, 3 k to 100 k) for 7 days. **A**, Representative Western blot of MYBPC3ic crude protein fractions stained for TTL and respective Ponceau. **B**, Quantification of TTL protein levels normalized to Ponceau and related to NT mean in MYBPC3ic hiPSC-CMs (n/d=3/1). MYBPC3ic and MYBPC3het hiPSC lines were differentiated into cardiomyocytes for 2 weeks and then transduced with AAV9-Empty or AAV9-TTL (MOI, 100 k) for 10 days in the presence of H_2O (control [ctrl]; **C–E**) or 100 nmol/L ET1 (endothelin-1; **F–H**) for the last 3 days. Representative immunofluorescence analysis of MYBPC3ic and MYBPC3het hiPSC-CMs transduced with AAV9-Empty or AAV9-TTL for 10 days in (**C**) basal condition or (**F**) after stimulation with ET1; hiPSC-CMs were stained for ACTN2 (α-actinin-2; purple), N-cadherin (N-Cad; green), and DAPI (4′,6-diamidino-2-phenylindole; blue). Scale bar=100 μm. Quantification of cell area in hiPSC-CMs (n/d=3/1) in (**D**) basal condition (N/n/d=758/3/1 [MYBPC3ic-Empty], 869/3/1 [MYBPC3ic-TTL], 336/3/1 [MYBPC3het-Empty], and 375/3/1 [MYBPC3het-TTL]) or (**G**) after stimulation with ET1 (N/n/d=705/3/1 [MYBPC3ic-Empty], 860/3/1 [MYBPC3ic-TTL], 210/3/1 [MYBPC3het-Empty], and 315/3/1 [MYBPC3het-TTL]). Selected hits of dysregulated RNA counts obtained with the nanostring analysis in (**E**) basal condition (ctrl) or (**H**) after stimulation with ET1 (N/n/d=9/3/3). Data are expressed as mean±SEM. Statistical significance was assessed with the Kruskal-Wallis test and Dunn multiple comparisons test. ns, $P>0.05$. N/n/d indicates number of cells/wells/differentiations; and NT, nontransduced.

and the sarcomere as the main enriched pathways in KI-Empty mice (Figure 6B; Data Set S2). On the contrary, no significant difference (P_{adj}>0.05) in protein levels was observed in KI-TTL versus KI-Empty mice (Figure 6B; Data Set S2), suggesting that TTL does not impact protein quantities in KI mice. MS analysis of the soluble protein fraction revealed 48 and 29 proteins that were higher and lower abundant in KI-Empty than in WT-Empty samples, respectively (Data Set S2). GO pathway analysis revealed cytoskeleton and the sarcomere as the main enriched pathways in KI-Empty versus WT-Empty mice (Figure S5A; Data Set S2). TTL and CYB5R1 (cytochrome b5 reductase 1) were the only proteins that exhibited significantly higher levels in KI-TTL than KI-Empty cytosolic fractions (Data Set S2).

Proteomic analysis of tubulins revealed an accumulation of most tubulin isoforms in the insoluble fractions of KI-Empty versus WT-Empty and no difference between KI-TTL and KI-Empty (Figure S5B; Data Set S2). TUBA4A and TUBA1C were the most abundant of the α-isoforms in the MS data set, showed higher level in KI-Empty than in WT-Empty, but did not differ between KI-TTL and KI-Empty, supporting data obtained by Western blot in the insoluble protein fraction (Figure 4C and 4D). Interestingly, tubulin mRNA and protein levels were inversely correlated in KI-Empty, that is, lower mRNA levels were associated with higher protein levels than in WT-Empty (Figure S5C). TTL induced accumulation of most tubulin mRNAs and had no significant impact on tubulin protein levels in KI mice (Figure S5D). Proteomic analysis also showed several tubulin isoforms in the cytosolic protein fraction and no difference in levels between the 3 groups (Data Set S2).

TTL Overexpression Rescues Hypertrophy in Cardiomyocytes Derived From an HCM hiPSC Line

To translate our mouse data to humans, we used a HCM patient–derived MYBPC3het (UKEi070-A) and MYBPC3ic (UKEi070-A1) hiPSC lines that were previously created.[13] MYBPC3het carries the c.2308G>A genetic variant (p.Asp770Serfs98X), resulting in MYBPC3 protein haploinsufficiency in cardiomyocytes.[13] We first evaluated the dose-response of AAV9-TTL in MYBPC3ic hiPSC-derived cardiomyocytes and found that an MOI of 100 000 gave rise to 19-fold higher TTL protein level than in nontransduced or AAV9-Empty–transduced cardiomyocytes (Figure 7A and 7B). We then evaluated the impact of a 10-day gene transfer of AAV9-TTL and AAV9-Empty (MOI, 100 000) in both genotypes in the presence of H_2O (control) or 100 nmol/L ET1 for the last 3 days (Figure 7C through 7H), as described previously.[26,45] In basal condition, mean cell area was 1.6-fold higher in MYBPC3het than in MYBPC3ic, and TTL overexpression normalized cell hypertrophy in both groups

(Figure 7C and 7D). ET1 induced cellular hypertrophy in MYBPC3ic and to a higher extent in MYBPC3het (3.4-fold higher than in MYBPC3ic), and AAV9-TTL normalized this effect in both groups (Figure 7F and 7G). These data revealed an antihypertrophic effect of TTL and activation of tubulin tyrosination in a human cellular model of HCM.

All groups were subjected to a gene expression analysis using the nanoString nCounter Elements technology and customized human-specific panels for heart failure, microtubules, and autophagy. In basal condition, some markers were higher (NPPA, S100A4, VASH1, TFEB, and MAPT), and markers of autophagy (MAP1LC3B and SQSTM1) and tubulin isoforms (TUBA1C, TUBB, TUBB4B, and TUBB6) were lower in MYBPC3het than in MYBPC3ic, but TTL effect was not clear (Figure 7E). In the presence of ET1, several markers were normalized in MYBPC3het with TTL, such as COL1A1, NPPA, MAPT, MTOR, MAP1LC3B, and SQSTM1 (Figure 7H).

Chronic Activation of Tubulin Tyrosination Improves Contractility in hiPSC-Derived EHTs

To evaluate the impact of chronic tubulin tyrosination or dTyr-tub in a human context, hiPSC lines deficient in SVBP or TTL were created from a WT hiPSC line (mTag-RFP-T-TUBA1B) with CRISPR/Cas9 genetic tools (Figure S2A through S2D) and differentiated into cardiomyocytes and maintained for 30 days in complete medium. Fluorescence-activated cell sorting (FACS) analysis revealed >90% TNNT2+ cells in the 3 groups (data not shown). RT-qPCR confirmed the respective deficiency of SVBP and TTL mRNAs in hiPSC-derived cardiomyocytes (Figure S2E and S2F). Analysis of mRNAs encoding sarcomeric proteins was performed on pooled RNAs from 30-day-old hiPSC-derived cardiomyocytes with the nanostring nCounter Elements technology and a customized human-specific sarcomere panel. Overall, no major difference was observed between the groups (Figure S6). These data suggest that sarcomerogenesis and cardiomyocyte differentiation are not affected by the deficiency of SVBP or TTL. SVBP-KO and TTL-KO hiPSC-derived cardiomyocytes, respectively, exhibited a markedly lower and higher dTyr-tub immunofluorescence intensity (Figure 8A) and protein levels (Figure 8B), confirming the targeting of either protein in hiPSC lines.

Then, EHTs from the 3 genotypes were cast either on standard posts (0.28 mN/mm) or on stiffer posts that enhance afterload (0.8 mN/mm) and were evaluated at the age of 60 days. On standard posts, force amplitude did not significantly differ between the groups, time to 50% peak was longer in SVBP-KO than in the other groups and did not differ to WT in TTL-KO (Figure 8C). Conversely, time from peak tension to 50% relaxation was longer in TTL-KO than in the other groups and did not differ to WT in SVBP-KO (Figure 8C). On stiffer
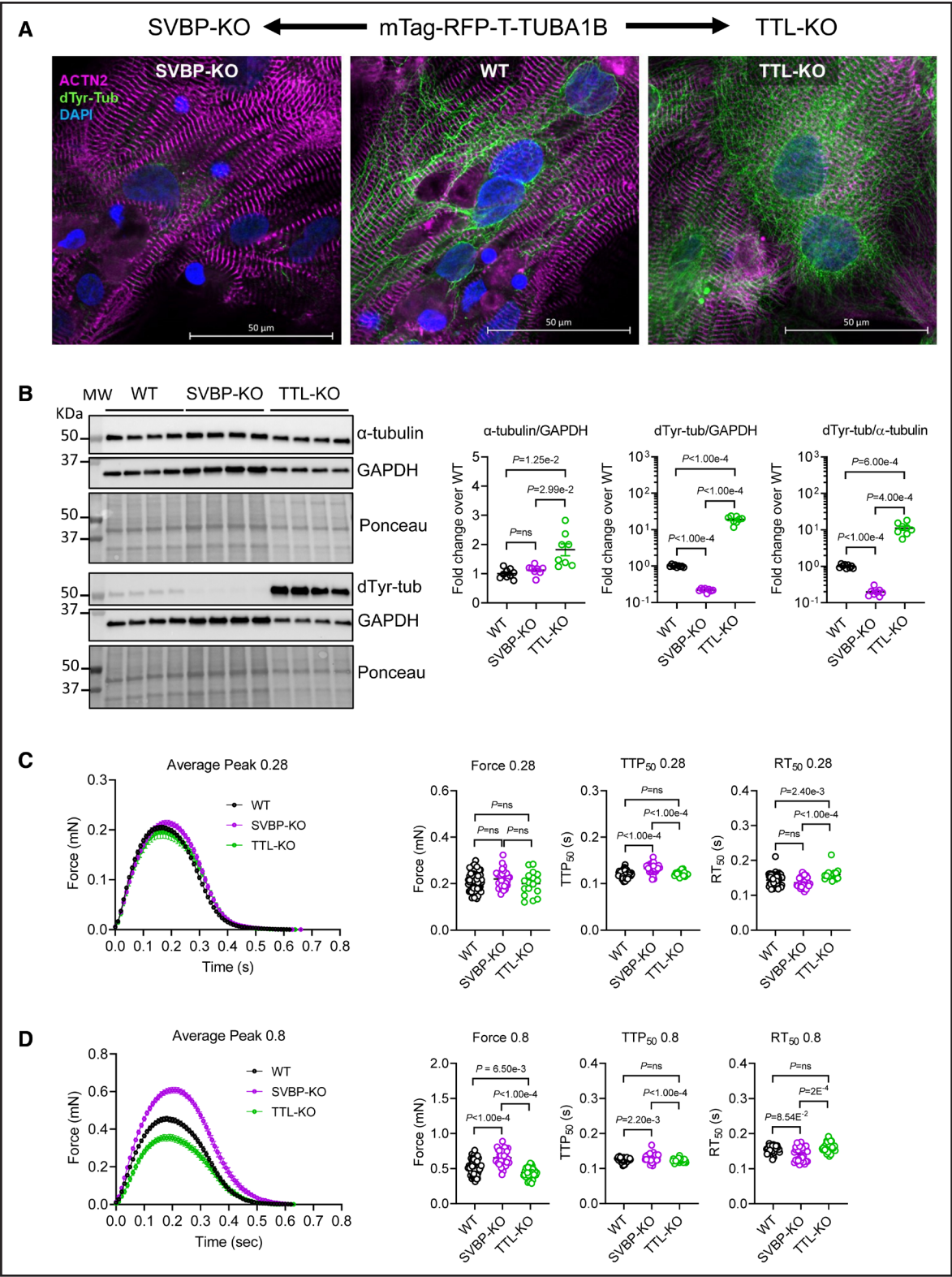
Figure 8. Evaluation of SVBP-KO and TTL-KO human induced pluripotent stem cell (hiPSC)–derived cardiomyocytes and engineered heart tissues (EHTs).

SVBP-KO and TTL-KO hiPSC lines were created from a control wild-type (WT) hiPSC line (mTag-RFP-T-TUBA1B [tubulin alpha 1b]) with CRISPR/Cas9 (clustered regularly interspaced short palindromic repeats/clustered regularly interspaced short palindromic repeat–associated protein 9) genetic tools and differentiated into cardiomyocytes and EHTs. **A**, Immunofluorescence analysis of 30-day-old SVBP-KO, WT, and TTL-KO hiPSC-derived cardiomyocytes stained for ACTN2 (α-actinin-2; purple), detyrosinated tubulin (dTyr-tub; green), and DAPI (4′,6-diamidino-2-phenylindole; blue). Scale bar=50 μm. **B**, Western blot was performed on crude protein fractions of 30-day-old hiPSC-derived cardiomyocytes and stained for α-tubulin, dTyr-tub, GAPDH, and Ponceau. Quantification of protein levels of α-tubulin/GAPDH, dTyr-tub/GAPDH, (*Continued*)

posts, force amplitude and time to 50% peak were significantly higher, whereas time from peak tension to 50% relaxation did not significantly differ in SVBP-KO than in WT (Figure 8D). In TTL-KO EHTs, force amplitude was lower and time to 50% peak was longer than in WT, time from peak tension to 50% relaxation did not significantly differ to WT and was markedly longer than in SVBP-KO (Figure 8D). Therefore, stiffer posts were required to reveal an opposite phenotype in SVBP-KO and TTL-KO. These findings provide evidence in a human cellular context that chronic tubulin tyrosination (=SVBP-KO) improved contractility in human EHTs, whereas chronic dTyr-tub (=TTL-KO) leads to contractility impairment.

RNA-seq and MS analyses were then performed in EHTs from WT on standard posts and on WT, SVBP-KO, and TTL-KO on stiff posts. GO analysis of RNA-seq data revealed that stiffer posts induced an enrichment (log2 ratio >0.58, P_{adj}<0.05) in components of mitochondria and of metabolic process, suggesting maturation in WT EHTs (Figure S7A; Data Set S3). SVBP-KO exhibited enrichment versus TTL-KO in components of extracellular matrix, endoplasmic reticulum, Golgi, plasma membrane, and sarcomere, associated with an enrichment in the developmental process, actin and cytoskeleton organization, and muscle contraction (Figure S7B; Data Set S3). Conversely, TTL-KO showed enrichment versus SVBP-KO in components of mitochondria, ribosome, RNA binding, associated with enrichment in the process of oxidative phosphorylation, mitochondrial electron transport, translation, and several other metabolic process (Figure S7C; Data Set S3).

GO analysis of MS data showed enrichment in components of extracellular exosomes, vesicles, and mitochondria in WT EHTs cast on stiffer posts (Figure S7D; Data Set S4). SVBP-KO exhibited enrichment versus TTL-KO in several cardiomyocyte components, including stress and contractile fibers, actin cytoskeleton, costamere, intracellular organelles, Z disc, and intercalated disc proteins, which were involved in cytoskeletal and actinin protein binding, actin filament-based process, muscle contraction, exocytosis, and gluconeogenesis (Figure S7E; Data Set S4). Conversely, GO analysis of TTL-KO showed enrichment versus SVBP-KO in components of the endoplasmic reticulum, Golgi, mitochondria, and secreted vesicles, which were involved in intracellular transport, metabolic process,

negative regulation of proteolysis, and response to stress (Figure S7F; Data Set S4).

DISCUSSION

This study evaluated the impact of chronic activation of tubulin tyrosination in WT and HCM mice, HCM hiPSC-derived cardiomyocytes, and in hiPSC-EHTs. The main findings are as follows: (1) a 6-week TTL overexpression dose dependently reduced dTyr-tub and improved cardiomyocyte contractility without affecting calcium transients in WT rodent cardiomyocytes; (2) long-term AAV9-TTL overexpression reduced dTyr-tub, improved diastolic filling, CO, and volumes, and reduced stiffness without impact on TTN isoform composition in KI mice; (3) AAV9-TTL gene transfer for 10 days normalized cell area in HCM hiPSC-derived cardiomyocytes; (4) TTL overexpression induced transcription of several tubulin isoforms and other structural components of the cytoskeleton but did not significantly impact the proteome in KI mice; (5) SVBP-deficient EHTs exhibited much lower dTyr-tub levels, higher force, and faster relaxation than in TTL-deficient EHTs under afterload; (6) RNA-seq and MS analyses revealed distinct enrichment of cardiomyocyte components and pathways in SVBP-KO and TTL-KO EHTs.

KI mice exhibited global cardiac dysfunction (CO, SV, and stroke work), abnormal systolic (EF) and diastolic relaxation (lower dP/dt$_{min}$, prolonged τ, and isovolumic relaxation time), and LV hypertrophy (higher LV mass/BW), as shown previously.[10,11,18] In addition, the expression of several genes involved in heart failure and autophagy-lysosomal pathway were dysregulated in KI mice, as reported previously.[44] Most tubulin isoforms exhibited lower mRNA and higher protein levels in KI mice, such as those observed in human heart failure samples.[46] Tubulin hyperstability in KI mice could be related to longer protein lifetimes and increased autoinhibition of tubulin mRNAs. This is consistent with the known tubulin autoregulation, characterized by mRNA repression by free tubulin protein in heart failure.[46] We also show that mRNA levels of several MAPs, such as dyneins, dynactins, kinesins, CLIPs, MAP isoforms, and MAPRE members are higher in KI than in WT mice. This suggests a broad upregulation of a microtubule transport program in KI mice. Proteomic analyses of insoluble and soluble protein fractions revealed higher abundance of sarcomeric, cytoskeletal, and intercalated disc proteins, such

Figure 8 Continued. and dTyr-tub/α-tubulin relative to WT mean; N/d=10/2 (WT), 8/2 (SBBP-KO), and 8/2 (TTL-KO). hiPSC-derived cardiomyocytes were cast in EHTs and cultivated for 60 days. Measurements of average peak, force amplitude, time to 50% of peak (TTP$_{50}$), and time to 50% relaxation (RT$_{50}$) of 60-day-old EHTs cast on (**C**) standard posts (0.28 mN/mm; N/d=75/6 [WT], 33/5 [SVBP-KO], and 17/2 [TTL-KO]) or on (**D**) afterload enhanced posts (0.8 mN/mm; N/d=54/6 [WT], 33/5 [SVBP-KO], and 38/5 [TTL-KO]). Data are expressed as mean±SEM. Statistical significance was assessed with Brown-Forsythe and Welch ANOVA test and Dunnett T3 multiple comparisons test (**B**) and with Kruskal-Wallis test and Dunn multiple comparisons test (**C** and **D**). ns, P>0.05. KO indicates knockout; N/d, number of samples/differentiations; SVBP, small vasohibin-binding protein; and TTL, tubulin tyrosine ligase.

as ANKRD1 (ankyrin repeat domain 1), DES (desmin), FHL1 (four and a half LIM domains 1), MYOM3 (myomesin 3), MYH7 (myosin heavy chain 7), NRAP (nebulin related anchoring protein), TCAP (titin-cap), XIRP1 (xin actin binding repeat containing 1), and XIRP2 (xin actin binding repeat containing 2, components of the proteasome such as PSMD14 (proteasome 26S subunit, non-ATPase 14), and several heat shock proteins in KI mice. These data suggest a stable, dTyr-MT network, providing a degree of viscoelastic resistance in KI myocardium. In the cytosolic fraction, there was no major difference in dTyr-tub, α-tubulin, and dTyr-tub/α-tubulin amounts between KI-Empty and WT-Empty, whereas in the insoluble protein fraction, dTyr-tub, α-tubulin, and dTyr-tub/α-tubulin levels were higher in KI-Empty than in WT-Empty, as previously shown.[3] Lowering dTyr-tub would be the priority therapeutic goal.

Chronic TTL overexpression dose dependently reduced the abundance of myocardial levels of dTyr-tub and dTyr-tub/α-tubulin but not of α-tubulin in neonatal and adult WT mice (Figure 1B; Figure S1D), supporting previous findings obtained acutely in human intact cardiomyocytes.[8,9] In KI mice, TTL increased the level of α-tubulin in the soluble but not in the insoluble protein fraction and markedly reduced the dTyr-tub level in the insoluble protein fraction, resulting in the normalization of dTyr-tub/α-tubulin. The remaining dTyr-tub after chronic TTL treatment in KI mice could be explained by the higher abundance of TUBA4A in KI mice, which is the only tubulin isoform translated as detyrosinated,[4,7] and of the detyrosinase MATCAP1,[43] but not by a transcriptional activation of the VASH1/SVBP complex (Figure 5F). GO pathway analysis of RNA-seq in KI-TTL versus KI-Empty revealed enrichment of structural components of the cytoskeleton and tubulins. On the contrary, TTL overexpression did not significantly affect the proteome, including tubulins in KI mice, except for the higher level in the soluble protein fraction of CYB5R1, which is involved in desaturation and elongation of fatty acids, cholesterol biosynthesis, and drug metabolism. We thus hypothesize that TTL-bound α/β-tubulin dimers in the cytosol will not trigger tubulin autoregulation and mRNA repression, leading to tubulin mRNA stabilization. While these findings are suggestive, we did not directly measure whether TTL overexpression alters autoregulation, which is a limitation of our study.

A 6-week in vivo AAV9-TTL administration reduced stiffness and improved fractional shortening and velocities of contraction and relaxation in a dose-dependent manner in cardiomyocytes isolated from WT rats. In HCM KI mice, chronic TTL therapy markedly increased diastolic filling and compliance, leading to improved global cardiac function (SV, CO, and stroke work). Increased compliance and reduced stiffness in KI-TTL mice was not associated with a shift of stiff-to-compliant TTN isoform in KI mice. In addition, TTL did not improve isovolumic

relaxation (dP/dt$_{min}$, τ, and isovolumic relaxation time) and had no impact on LV hypertrophy in KI mice. We, therefore, suggest that the absence of TTL effect on isovolumic relaxation in KI mice in vivo is maybe intrinsic to the model, which exhibited a low level of MYBPC3.[10] Indeed, it was previously shown that MYBPC3, besides its role in maintaining the super-relaxed state of myosin and full relaxation in diastole,[47–50] plays also a role in sustaining LV systolic stiffening.[51] This is supported by the lower aortic ejection time in KI mice (Table S2), the faster contractility in EHTs derived from *Mybpc3*-KO and KI neonatal mice,[52,53] and by the higher rates of the early fast-exponential phase of relaxation measured in human HCM septal myectomy with MYBPC3 haploinsufficiency.[54] Therefore, we propose a model in which TTL markedly improves diastolic filling and compliance to compensate the abnormal relaxation deficit intrinsic to the KI mouse model, leading to improved global cardiac function.

Interestingly, a 10-day TTL treatment normalized cellular hypertrophy and partially corrected the hypertrophic transcriptome in human HCM cardiomyocytes. The positive impact of chronic TTL overexpression on global heart function was supported by the findings obtained in hiPSC-derived cardiomyocytes and EHTs deficient in either SVBP or TTL. Knockout of these genes in hiPSCs did not affect cardiomyocyte differentiation as evidenced by similar high percentage of TNNT2+ cells and expression pattern of sarcomeric genes. Instead, this study shows markedly lower level of dTyr-tub and dTyr-tub/α-tubulin, higher force of contraction, and faster relaxation in SVBP-KO than in TTL-KO hiPSC-derived cardiomyocytes and EHTs, which was not the consequence of increased sarcomerogenesis and cardiomyocyte differentiation. Conversely, the TTL-KO cardiomyocytes and EHTs showed much higher levels of dTyr-tub and dTyr-tub/α-tubulin, lower force of contraction, and prolonged relaxation. These data provide evidence in a human cellular context that chronic activation of tubulin tyrosination (=SVBP-KO) improved contractility in human EHTs, whereas chronic activation of tubulin detyrosination (=TTL-KO) induced contractility impairment, mimicking the situation in several types of heart failure[2,3] (for reviews, see references[4–7]). Contractility findings in SVBP-KO EHTs were supported by the RNA-seq and proteomic analyses, showing enrichment in components involved in muscle structure development, response to stimulus, cytoskeleton binding and function, and muscle contraction, whereas TTL-KO EHTs were rather enriched in components involved in oxidative phosphorylation, mitochondrial electron transport, translation, mRNA degradation, response to stress and other metabolic processes.

Our study supports previous findings obtained after acute treatment with either TTL treatment in isolated intact failing cardiomyocytes[8,9] or with a VASH inhibitor

in a rat model of heart failure with preserved EF.[55] We provide evidence that a chronic AAV9-TTL application improves diastolic filling and compliance leading to better global cardiac function in HCM mice and normalized cellular hypertrophy in HCM hiPSC-derived cardiomyocytes. AAV9-based therapy has been tested in mouse or human cellular models of HCM (*MYBPC3*) and arrhythmogenic cardiomyopathy (*PKP2*). Long-term AAV9-*MYBPC3* therapy prevented the development of the cardiomyopathic phenotype in *Mybpc3*-deficient mice[18] and normalized cellular hypertrophy in HCM hiPSC-derived cardiomyocytes.[56] Similarly, *PKP2* gene therapy reduced ventricular arrhythmias, reversed remodeling of the right ventricle, improved heart function, and extended survival in a *Pkp2*-deficient mouse model of arrhythmogenic cardiomyopathy.[57] We are aware that AAV9 also targets the liver and could induce some liver toxicity,[58] and the combination of AAV9 and a CMV promoter resulted in a lower detection of GFP in the mouse liver.[17] On the other hand, the combination of AAV9 and the human cardiomyocyte-specific promoter *TNNT2* limits the expression of the *Mybpc3* transgene to the cardiomyocytes and not in the liver in mice.[18] There are currently no results of clinical trials using AAV9-mediated gene therapy for cardiomyopathies, although a phase 1b trial with AAV9-*MYBPC3* for patients with HCM (https://www.clinicaltrials.gov; unique identifier: NCT05836259) and a phase 2 trial with AAV9-*LAMP2B* for patients with Danon disease (https://www.clinicaltrials.gov; unique identifier: NCT06092034) have started.

In conclusion, this study provides the first proof of concept that chronic activation of tubulin tyrosination in HCM mice and in human EHTs improves heart function and holds promise for targeting the nonsarcomeric cytoskeleton in heart disease.

ARTICLE INFORMATION

Affiliations

Department of Experimental Pharmacology and Toxicology (N.P., B.G., E.K., G.M., S.S., L.C.), Department of Cardiology, University Heart and Vascular Center (S.K., L.B., D.W., D.L.), Section Mass Spectrometric Proteomics (B.S., H.V., H.S.), and Vector Facility, Department of Experimental Pharmacology and Toxicology (I.B.), University Medical Center Hamburg-Eppendorf, Hamburg, Germany. Now with Institute of Experimental Cardiovascular Research, University Medical Center Hamburg-Eppendorf, Germany (S.K.). Now with Faculty of Medicine, Department of Cardiology and Angiology, University Heart Center Freiburg-Bad Krozingen, University of Freiburg, Germany (L.B., D.W., D.L.). German Centre for Cardiovascular Research (DZHK), Partner Site Hamburg/Kiel/Lübeck, Germany (N.P., D.W., G.M., S.S., D.L., L.C.). Department of Physiology, Pennsylvania Muscle Institute, University of Pennsylvania Perelman School of Medicine, Philadelphia, PA (C.Y.C., M.A.C., B.L.P.). Now with Gene Therapy Program, Department of Medicine, Perelman School of Medicine, University of Pennsylvania, Philadelphia, PA (C.Y.C.). Now with Department of Molecular Physiology and Biophysics, University of Vermont Larner College of Medicine, Burlington, VT (M.A.C.). Department of Genetic Epidemiology, Institute of Human Genetics, University of Münster, Germany (M.H.-R.). Joint Institute for Individualisation in a Changing Environment, University of Münster and Bielefeld University, Münster, Germany (M.H.-R.). Amsterdam University Medical Center, Vrije Universiteit Amsterdam, Department of Physiology, Amsterdam Cardiovascular Sciences, Amsterdam, the Netherlands (J.v.d.V.).

REFERENCES

1. Carrier L. Targeting the population for gene therapy with MYBPC3. *J Mol Cell Cardiol.* 2021;150:101–108. doi: 10.1016/j.yjmcc.2020.10.003

2. Robison P, Caporizzo MA, Ahmadzadeh H, Bogush AI, Chen CY, Margulies KB, Shenoy VB, Prosser BL. Detyrosinated microtubules buckle and bear load in contracting cardiomyocytes. *Science.* 2016;352:aaf0659. doi: 10.1126/science.aaf0659

3. Schuldt M, Pei J, Harakalova M, Dorsch LM, Schlossarek S, Mokry M, Knol JC, Pham TV, Schelfhorst T, Piersma SR, et al. Proteomic and functional studies reveal detyrosinated tubulin as treatment target in sarcomere mutation-induced hypertrophic cardiomyopathy. *Circ Heart Fail.* 2021;14:e007022. doi: 10.1161/CIRCHEARTFAILURE.120.007022

4. Sanyal C, Pietsch N, Ramirez Rios S, Peris L, Carrier L, Moutin MJ. The detyrosination/re-tyrosination cycle of tubulin and its role and dysfunction in neurons and cardiomyocytes. *Semin Cell Dev Biol.* 2023;137:46–62. doi: 10.1016/j.semcdb.2021.12.006

5. Caporizzo MA, Chen CY, Prosser BL. Cardiac microtubules in health and heart disease. *Exp Biol Med (Maywood).* 2019;244:1255–1272. doi: 10.1177/1535370219868960

6. Caporizzo MA, Prosser BL. The microtubule cytoskeleton in cardiac mechanics and heart failure. *Nat Rev Cardiol.* 2022;19:364–378. doi: 10.1038/s41569-022-00692-y

7. Uchida K, Scarborough EA, Prosser BL. Cardiomyocyte microtubules: control of mechanics, transport, and remodeling. *Annu Rev Physiol.* 2022;84:257–283. doi: 10.1146/annurev-physiol-062421-040656

8. Chen CY, Caporizzo MA, Bedi K, Vite A, Bogush AI, Robison P, Heffler JG, Salomon AK, Kelly NA, Babu A, et al. Suppression of detyrosinated microtubules improves cardiomyocyte function in human heart failure. *Nat Med.* 2018;24:1225–1233. doi: 10.1038/s41591-018-0046-2

9. Chen CY, Salomon AK, Caporizzo MA, Curry S, Kelly NA, Bedi K, Bogush AI, Kramer E, Schlossarek S, Janiak P, et al. Depletion of vasohibin 1 speeds contraction and relaxation in failing human cardiomyocytes. *Circ Res.* 2020;127:e14–e27. doi: 10.1161/CIRCRESAHA.119.315947

10. Vignier N, Schlossarek S, Fraysse B, Mearini G, Kramer E, Pointu H, Mougenot N, Guiard J, Reimer R, Hohenberg H, et al. Nonsense-mediated mRNA decay and ubiquitin-proteasome system regulate cardiac myosin-binding protein C mutant levels in cardiomyopathic mice. *Circ Res.* 2009;105:239–248. doi: 10.1161/CIRCRESAHA.109.201251

11. Fraysse B, Weinberger F, Bardswell SC, Cuello F, Vignier N, Geertz B, Starbatty J, Kramer E, Coirault C, Eschenhagen T, et al. Increased

myofilament Ca(2+) sensitivity and diastolic dysfunction as early consequences of Mybpc3 mutation in heterozygous knock-in mice. *J Mol Cell Cardiol.* 2012;52:1299–1307. doi: 10.1016/j.yjmcc.2012.03.009

12. Perez-Riverol Y, Bai J, Bandla C, Garcia-Seisdedos D, Hewapathirana S, Kamatchinathan S, Kundu DJ, Prakash A, Frericks-Zipper A, Eisenacher M, et al. The PRIDE database resources in 2022: a hub for mass spectrometry-based proteomics evidences. *Nucleic Acids Res.* 2022;50:D543–D552. doi: 10.1093/nar/gkab1038

13. Warnecke N, Ulmer BM, Laufer SD, Shibamiya A, Kramer E, Neuber C, Hanke S, Behrens C, Loos M, Munch J, et al. Generation of bi-allelic MYBPC3 truncating mutant and isogenic control from an iPSC line of a patient with hypertrophic cardiomyopathy. *Stem Cell Res.* 2021;55:102489. doi: 10.1016/j.scr.2021.102489

14. Lock M, McGorray S, Auricchio A, Ayuso E, Beecham EJ, Blouin-Tavel V, Bosch F, Bose M, Byrne BJ, Caton T, et al. Characterization of a recombinant adeno-associated virus type 2 reference standard material. *Hum Gene Ther.* 2010;21:1273–1285. doi: 10.1089/hum.2009.223

15. Lock M, Alvira MR, Chen SJ, Wilson JM. Absolute determination of single-stranded and self-complementary adeno-associated viral vector genome titers by droplet digital PCR. *Hum Gene Ther Methods.* 2014;25:115–125. doi: 10.1089/hgtb.2013.131

16. Mearini G, Stimpel D, Kramer E, Geertz B, Braren I, Gedicke-Hornung C, Precigout G, Muller OJ, Katus HA, Eschenhagen T, et al. Repair of Mybpc3 mRNA by 5'-trans-splicing in a mouse model of hypertrophic cardiomyopathy. *Mol Ther Nucleic Acids.* 2013;2:e102. doi: 10.1038/mtna.2013.31

17. Gedicke-Hornung C, Behrens-Gawlik V, Reischmann S, Geertz B, Stimpel D, Weinberger F, Schlossarek S, Precigout G, Braren I, Eschenhagen T, et al. Rescue of cardiomyopathy through U7snRNA-mediated exon skipping in Mybpc3-targeted knock-in mice. *EMBO Mol Med.* 2013;5:1128–1145. doi: 10.1002/emmm.201202168

18. Mearini G, Stimpel D, Geertz B, Weinberger F, Krämer E, Schlossarek S, Mourot-Filiatre J, Stöhr A, Dutshc A, Wijnker PJM, et al. Mybpc3 gene therapy for neonatal cardiomyopathy enables longterm disease prevention in mice. *Nat Commun.* 2014;5:5515. doi: 10.1038/ncomms6515

19. Kerr JP, Robison P, Shi G, Bogush AI, Kempema AM, Hexum JK, Becerra N, Harki DA, Martin SS, Raiteri R, et al. Detyrosinated microtubules modulate mechanotransduction in heart and skeletal muscle. *Nat Commun.* 2015;6:8526. doi: 10.1038/ncomms9526

20. Caporizzo MA, Chen CY, Salomon AK, Margulies KB, Prosser BL. Microtubules provide a viscoelastic resistance to myocyte motion. *Biophys J.* 2018;115:1796–1807. doi: 10.1016/j.bpj.2018.09.019

21. Concordet JP, Haeussler M. CRISPOR: intuitive guide selection for CRISPR/Cas9 genome editing experiments and screens. *Nucleic Acids Res.* 2018;46:W242–W245. doi: 10.1093/nar/gky354

22. Mosqueira D, Mannhardt I, Bhagwan JR, Lis-Slimak K, Katili P, Scott E, Hassan M, Prondzynski M, Harmer SC, Tinker A, et al. CRISPR/Cas9 editing in human pluripotent stem cell-cardiomyocytes highlights arrhythmias, hypocontractility, and energy depletion as potential therapeutic targets for hypertrophic cardiomyopathy. *Eur Heart J.* 2018;39:3879–3892. doi: 10.1093/eurheartj/ehy249

23. Prondzynski M, Lemoine MD, Zech AT, Horvath A, Di Mauro V, Koivumaki JT, Kresin N, Busch J, Krause T, Kramer E, et al. Disease modeling of a mutation in alpha-actinin 2 guides clinical therapy in hypertrophic cardiomyopathy. *EMBO Mol Med.* 2019;11:e11115. doi: 10.15252/emmm.201911115

24. Rhoden A, Schulze T, Pietsch N, Christ T, Hansen A, Eschenhagen T. Comprehensive analyses of the inotropic compound omecamtiv mecarbil in rat and human cardiac preparations. *Am J Physiol Heart Circ Physiol.* 2022;322:H373–H385. doi: 10.1152/ajpheart.00534.2021

25. Zech ATL, Prondzynski M, Singh SR, Pietsch N, Orthey E, Alizoti E, Busch J, Madsen A, Behrens CS, Meyer-Jens M, et al. ACTN2 mutant causes proteopathy in human iPSC-derived cardiomyocytes. *Cells.* 2022;11:2745. doi: 10.3390/cells11172745

26. Meyer-Jens M, Wenzel K, Grube K, Rüdebusch J, Krämer E, Bahls M, Müller K, Voß H, Schlüter H, Felix SB, Carrier L, Könemann S, Schlossarek S. Sacubitril/valsartan reduces proteasome activation and cardiomyocyte area in an experimental mouse model of hypertrophy. *J Mol Cell Cardiol Plus.* 2024;7:100059. doi: 10.1016/j.jmccpl.2023.100050

27. Pacher P, Nagayama T, Mukhopadhyay P, Batkai S, Kass DA. Measurement of cardiac function using pressure-volume conductance catheter technique in mice and rats. *Nat Protoc.* 2008;3:1422–1434. doi: 10.1038/nprot.2008.138

28. Hinrichs S, Scherschel K, Kruger S, Neumann JT, Schwarzl M, Yan I, Warnke S, Ojeda FM, Zeller T, Karakas M, et al. Precursor proadrenomedullin influences cardiomyocyte survival and local inflammation related to myocardial infarction. *Proc Natl Acad Sci USA.* 2018;115:E8727–E8736. doi: 10.1073/pnas.1721635115

29. Bacmeister L, Segin S, Medert R, Lindner D, Freichel M, Camacho Londoño JE. Assessment of PEEP-ventilation and the time point of parallel-conductance determination for pressure-volume analysis under beta-adrenergic stimulation in mice. *Front Cardiovasc Med.* 2019;6:36. doi: 10.3389/fcvm.2019.00036

30. Aillaud C, Bosc C, Peris L, Bosson A, Heemeryck P, Van Dijk J, Le Friec J, Boulan B, Vossier F, Sanman LE, et al. Vasohibins/SVBP are tubulin carboxypeptidases (TCPs) that regulate neuron differentiation. *Science.* 2017;358:1448–1453. doi: 10.1126/science.aao4165

31. Warren CM, Jordan MC, Roos KP, Krzesinski PR, Greaser ML. Titin isoform expression in normal and hypertensive myocardium. *Cardiovasc Res.* 2003;59:86–94. doi: 10.1016/s0008-6363(03)00328-6

32. Multhaup A, Huppertz B, Gohner C, Bohringer M, Mai M, Markert U, Schleussner E, Groten T. N-cadherin knockdown leads to disruption of trophoblastic and endothelial cell interaction in a 3D cell culture model - New insights in trophoblast invasion failure. *Cell Adh Migr.* 2018;12:259–270. doi: 10.1080/19336918.2017.1386822

33. Bolger AM, Lohse M, Usadel B. Trimmomatic: a flexible trimmer for Illumina sequence data. *Bioinformatics.* 2014;30:2114–2120. doi: 10.1093/bioinformatics/btu170

34. Kim D, Paggi JM, Park C, Bennett C, Salzberg SL. Graph-based genome alignment and genotyping with HISAT2 and HISAT-genotype. *Nat Biotechnol.* 2019;37:907–915. doi: 10.1038/s41587-019-0201-4

35. Li H, Handsaker B, Wysoker A, Fennell T, Ruan J, Homer N, Marth G, Abecasis G, Durbin R; 1000 Genome Project Data Processing Subgroup. The sequence alignment/map format and SAMtools. *Bioinformatics.* 2009;25:2078–2079. doi: 10.1093/bioinformatics/btp352

36. Anders S, Pyl PT, Huber W. HTSeq--a Python framework to work with high-throughput sequencing data. *Bioinformatics.* 2015;31:166–169. doi: 10.1093/bioinformatics/btu638

37. Love MI, Huber W, Anders S. Moderated estimation of fold change and dispersion for RNA-seq data with DESeq2. *Genome Biol.* 2014;15:550. doi: 10.1186/s13059-014-0550-8

38. Raudvere U, Kolberg L, Kuzmin I, Arak T, Adler P, Peterson H, Vilo J. g:Profiler: a web server for functional enrichment analysis and conversions of gene lists (2019 update). *Nucleic Acids Res.* 2019;47:W191–W198. doi: 10.1093/nar/gkz369

39. Hughes CS, Moggridge S, Muller T, Sorensen PH, Morin GB, Krijgsveld J. Single-pot, solid-phase-enhanced sample preparation for proteomics experiments. *Nat Protoc.* 2019;14:68–85. doi: 10.1038/s41596-018-0082-x

40. Tyanova S, Temu T, Sinitcyn P, Carlson A, Hein MY, Geiger T, Mann M, Cox J. The Perseus computational platform for comprehensive analysis of (prote)omics data. *Nat Methods.* 2016;13:731–740. doi: 10.1038/nmeth.3901

41. Wu T, Hu E, Xu S, Chen M, Guo P, Dai Z, Feng T, Zhou L, Tang W, Zhan L, Fu X, Liu S, Bo X, Yu G. clusterProfiler 4.0: a universal enrichment tool for interpreting omics data. *Innovation (Camb).* 2021;2:100141. doi: 10.1016/j.xinn.2021.100141

42. Salomon AK, Phyo SA, Okami N, Heffler J, Robison P, Bogush AI, Prosser BL. Desmin intermediate filaments and tubulin detyrosination stabilize growing microtubules in the cardiomyocyte. *Basic Res Cardiol.* 2022;117:53. doi: 10.1007/s00395-022-00962-3

43. Landskron L, Bak J, Adamopoulos A, Kaplani K, Moraiti M, van den Hengel LG, Song JY, Bleijerveld OB, Nieuwenhuis J, Heidebrecht T, et al. Posttranslational modification of microtubules by the MATCAP detyrosinase. *Science.* 2022;376:eabn6020. doi: 10.1126/science.abn6020

44. Singh SR, Zech ATL, Geertz B, Reischmann-Dusener S, Osinska H, Prondzynski M, Kramer E, Meng Q, Redwood C, van der Velden J, et al. Activation of autophagy ameliorates cardiomyopathy in Mybpc3-targeted knockin mice. *Circ Heart Fail.* 2017;10:e004140. doi: 10.1161/CIRCHEARTFAILURE.117.004140

45. Johansson M, Ulfenborg B, Andersson CX, Heydarkhan-Hagvall S, Jeppsson A, Sartipy P, Synnergren J. Cardiac hypertrophy in a dish: a human stem cell based model. *Biol Open.* 2020;9:bio052381. doi: 10.1242/bio.052381

46. Phyo SA, Uchida K, Chen CY, Caporizzo MA, Bedi K, Griffin J, Margulies K, Prosser BL. Transcriptional, post-transcriptional, and post-translational mechanisms rewrite the tubulin code during cardiac hypertrophy and failure. *Front Cell Dev Biol.* 2022;10:837486. doi: 10.3389/fcell.2022.837486

47. Pohlmann L, Kroger J, Vignier N, Schlossarek S, Kramer E, Coirault C, Sultan KR, El-Armouche A, Winegrad S, Eschenhagen T, Carrier L. Cardiac myosin-binding protein C is required for complete relaxation in intact myocytes. *Circ Res.* 2007;101:928–938. doi: 10.1161/CIRCRESAHA.107.158774

48. McNamara JW, Li A, Lal S, Bos JM, Harris SP, van der Velden J, Ackerman MJ, Cooke R, Dos Remedios CG, van der Velden J, et al. MYBPC3

ORIGINAL RESEARCH

mutations are associated with a reduced super-relaxed state in patients with hypertrophic cardiomyopathy. *PLoS One*. 2017;12:e0180064. doi: 10.1371/journal.pone.0180064

49. McNamara JW, Li A, Smith NJ, Lal S, Graham RM, Kooiker KB, van Dijk SJ, Remedios CGD, Harris SP, Cooke R. Ablation of cardiac myosin binding protein-C disrupts the super-relaxed state of myosin in murine cardiomyocytes. *J Mol Cell Cardiol*. 2016;94:65–71. doi: 10.1016/j.yjmcc.2016.03.009

50. Toepfer CN, Wakimoto H, Garfinkel AC, McDonough B, Liao D, Jiang J, Tai AC, Gorham JM, Lunde IG, Lun M, et al. Hypertrophic cardiomyopathy mutations in MYBPC3 dysregulate myosin. *Sci Transl Med*. 2019;11:eaat1199. doi: 10.1126/scitranslmed.aat1199

51. Palmer BM, Georgakopoulos D, Janssen PM, Wang Y, Alpert NR, Belardi DF, Harris SP, Moss RL, Burgon PG, Seidman CE, et al. Role of cardiac myosin binding protein C in sustaining left ventricular systolic stiffening. *Circ Res*. 2004;94:1249–1255. doi: 10.1161/01.RES.0000126898.95550.31

52. de Lange WJ, Grimes AC, Hegge LF, Ralphe JC. Ablation of cardiac myosin-binding protein-C accelerates contractile kinetics in engineered cardiac tissue. *J Gen Physiol*. 2013;141:73–84. doi: 10.1085/jgp.201210837

53. Stohr A, Friedrich FW, Flenner F, Geertz B, Eder A, Schaaf S, Hirt MN, Uebeler J, Schlossarek S, Carrier L, et al. Contractile abnormalities and altered drug response in engineered heart tissue from Mybpc3-targeted knock-in mice. *J Mol Cell Cardiol*. 2013;63:189–198. doi: 10.1016/j.yjmcc.2013.07.011

54. Pioner JM, Racca AW, Klaiman JM, Yang KC, Guan X, Pabon L, Muskheli V, Zaunbrecher R, Macadangdang J, Jeong MY, et al. Isolation and mechanical measurements of myofibrils from human induced pluripotent stem cell-derived cardiomyocytes. *Stem Cell Rep*. 2016;6:885–896. doi: 10.1016/j.stemcr.2016.04.006

55. Eaton DM, Lee BW, Caporizzo MA, Iyengar A, Chen CY, Uchida K, Marcellin G, Lannay Y, Vite A, Bedi KC Jr, et al. Vasohibin inhibition improves myocardial relaxation in a rat model of heart failure with preserved ejection fraction. *Sci Transl Med*. 2024;16:eadm8842. doi: 10.1126/scitranslmed.adm8842

56. Prondzynski M, Kramer E, Laufer SD, Shibamiya A, Pless O, Flenner F, Muller OJ, Munch J, Redwood C, Hansen A, et al. Evaluation of MYBPC3 trans-splicing and gene replacement as therapeutic options in human iPSC-derived cardiomyocytes. *Mol Ther Nucleic Acids*. 2017;7:475–486. doi: 10.1016/j.omtn.2017.05.008

57. Bradford W, Liang J, Mataraarachchi N, Do A, Gu Y, Peterson K, Sheikh F. Plakophilin-2 gene therapy prevents arrhythmogenic right ventricular cardiomyopathy development in a novel mouse model harboring patient genetics. *Nat Cardiovasc Res*. 2023;2:1246–1261. doi: 10.1038/s44161-023-00370-3

58. Chand D, Mohr F, McMillan H, Tukov FF, Montgomery K, Kleyn A, Sun R, Tauscher-Wisniewski S, Kaufmann P, Kullak-Ublick G. Hepatotoxicity following administration of onasemnogene abeparvovec (AVXS-101) for the treatment of spinal muscular atrophy. *J Hepatol*. 2021;74:560–566. doi: 10.1016/j.jhep.2020.11.001